JOURNAL OF PETROLOGY | VOLUME 37 | NUMBER 3 | PAGES 609–635 | 1996

DANTE CANIL* AND HUGH ST. C. O'NEILL†
BAYERISCHES GEOINSTITUT, UNIVERSITÄT BAYREUTH, D-95440 BAYREUTH, GERMANY

Distribution of Ferric Iron in some Upper-Mantle Assemblages

The distribution of ferric iron among the phases of upper-mantle rocks, as a function of pressure (P), temperature (T) and bulk composition, has been studied using ^{57}Fe Mössbauer spectroscopy to determine the $Fe^{3+}/\Sigma Fe$ ratios of mineral separates from 35 peridotite and pyroxenite samples. The whole-rock Fe^{3+} complement of a peridotite is typically shared approximately evenly among the major anhydrous phases (spinel and/or garnet, orthopyroxene and clinopyroxene), with the important exception of olivine, which contains negligible Fe^{3+}. Whole-rock Fe^{3+} contents are independent of the T and P of equilibration of the rock, but show a well-defined simple inverse correlation with the degree of depletion in a basaltic component. Fe^{3+} in spinel and in both pyroxenes from the spinel lherzolite facies shows a positive correlation with temperature, presumably owing to the decrease in the modal abundance of spinel. In garnet peridotites, the Fe^{3+} in garnet increases markedly with increasing T and P, whereas that in clinopyroxene remains approximately constant. The complex nature of the partitioning of Fe^{3+} between mantle phases results in complicated patterns of the activities of the Fe^{3+}-bearing components, and thus in calculated equilibrium f_{O_2}, which show little correlation with whole-rock Fe^{3+} or degree of depletion. Whether Fe^{3+} is taken into account or ignored in calculating mineral formulae for geothermobarometry can have major effects on the resulting calculated T and P. For Fe–Mg exchange geothermometers, large errors must occur when applied to samples more oxidized or reduced than the experimental calibrations, whose f_{O_2} conditions are largely unknown. Two-pyroxene thermometry is more immune to this problem, and probably provides the most reliable P–T estimates. Accordingly, the convergence of P–T values derived for a given garnet peridotite assemblage may not necessarily be indicative of mineral equilibrium. The prospects for the calculation of accurate Fe^{3+} contents from electron microprobe analyses by assuming stoichiometry are good for spinel, uncertain for garnet, and distinctly poor for pyroxenes.

KEY WORDS: *mantle; oxidation; partitioning; peridotite; thermobarometry*

*Corresponding author. Present address: School of Earth and Ocean Sciences, University of Victoria, P.O. Box 1700, Victoria, B.C., V8W 2Y2, Canada
†Present address: Research School of Earth Sciences, Australian National University, Canberra, A.C.T. 0200, Australia

INTRODUCTION

The accurate measurement of Fe^{3+} contents in upper-mantle minerals has been an area of much interest, mainly in an effort to calculate oxygen fugacities for mantle-derived rocks from equilibria involving Fe^{3+}-bearing components in spinel, garnet or clinopyroxene (Wood & Virgo, 1989; Dyar *et al.*, 1989, 1992; Canil *et al.*, 1990; Luth *et al.*, 1990; McGuire *et al.*, 1991; Luth & Canil, 1993). Although several investigations have presented quantitative Fe^{3+} contents for upper-mantle spinels, garnets and pyroxenes, few have examined in any detail the distribution of Fe^{3+} between these coexisting phases in upper-mantle rocks. McGuire *et al.* (1991) and Dyar *et al.* (1992) studied the distribution of Fe^{3+} amongst coexisting phases in one spinel lherzolite sample, and Dyar *et al.* (1989) performed a similar investigation for a suite of spinel lherzolite samples that equilibrated over a limited range of P–T–f_{O_2} conditions. Because of this minimal amount of data, very little is known about the factors responsible for the distribution of Fe^{3+} among upper-mantle phases, such as mineral or bulk (whole-rock) compositions, P and T. This distribution is important as it determines the concentrations, and hence activities, of Fe^{3+}-bearing components (e.g. Fe_3O_4 in spinel), and consequently the equilibrium f_{O_2} of any mantle assemblage.

In this study, the Fe^{3+} contents of coexisting pyroxenes (both ortho- and clino-), spinels and garnets from several well-characterized mantle-derived rocks are determined with ^{57}Fe Mössbauer spectroscopy. These and previously published data are used to examine partitioning systematics for Fe^{3+} between mantle phases in both the spinel and garnet lherzolite facies, and to evaluate the effect of Fe^{3+} on geothermobarometers applied to garnet peridotites.

SAMPLES

The samples selected represent a broad range in geochemistry, mineralogy and tectonic setting (Table 1). Original references to petrographic descriptions, and to bulk-rock and individual mineral chemical analyses (plus other details of sample sizes and analytical methods) are listed in Table 1. Bulk-rock and individual mineral chemical analyses are summarized in Table 2. Modal abundances and whole-rock Fe_2O_3 contents for these samples were reported by Canil *et al.* (1994).

Southeastern Australia

Five xenoliths from a number of Tertiary localities in this alkaline province were chosen. Two of the samples are modally metasomatized, containing phlogopite or amphibole. Detailed studies of their major and trace element geochemistry have been presented by Frey & Green (1974), McDonough & McCulloch (1987) and W. F. McDonough (unpublished data, 1993).

Northern Tanzania

These xenoliths are from the Pleistocene Olmani and Lashaine cinder cones. The samples include spinel and garnet peridotites, and Mg-rich dunites and wehrlites, the latter showing petrographic and geochemical evidence for carbonatite metasomatism (Rudnick *et al.*, 1993). Extended descriptions of their petrography, and major and trace element geochemistry and mineralogy have been given by Rudnick *et al.* (1992, 1993).

Southern Africa

Both low- and high-temperature peridotites (Boyd & Mertzman, 1987) hosted in late Precambrian to Cretaceous kimberlites emplaced in the Kaapvaal craton were studied. Some of the samples are graphite or diamond bearing and their geochemistry and/or mineral chemistry have been described previously (Shee *et al.*, 1982; Boyd & Mertzman, 1987; Viljoen *et al.*, 1992; Boyd *et al.*, 1993; Pearson *et al.*, 1994).

Siberia

These samples are from the Udachnaya kimberlite pipe (~350 Ma) in Siberia. Of particular interest is the common occurrence of diamond in several xenoliths from this locality (Pokhilenko *et al.*, 1991). The samples are one high- and low-temperature peridotite, and a number of small (<3 cm diameter) megacrystalline diamond-bearing garnet dunites. Mineralogical and isotopic studies of these samples are in progress by F. R. Boyd and coworkers (Boyd *et al.*, 1993; Pearson *et al.*, 1995).

Norway

Two garnet pyroxenite samples from the Ugelvik and Raudhaugene localities occur as lenses in Mg–Cr type garnet peridotites within the Western Gneiss Region described by Carswell (1986). These samples originated in the upper mantle, but have had a complex multi-stage metamorphic history during their emplacement into the crust (Jamtveit *et al.*, 1991).

Morocco

Garnets from two garnet pyroxenite layers (one graphite bearing and one graphite free) within the Beni Boussera peridotite massif, Morocco (Pearson *et al.*, 1993) were studied. These pyroxenite layers are thought to have formed originally in the diamond-stability field within the upper mantle (Pearson *et al.*, 1993).

ANALYTICAL METHODS

Minerals were separated from each sample using heavy liquid and/or magnetic techniques. Separates from this process were washed in dilute HCl or HF, and hand picked to optical purity under a binocular microscope. The amount of sample produced after this process varied from ~30 to 150 mg depending on the amount of bulk sample present. For some of the samples, a sufficient amount of clean separate could not be obtained for some phases (especially orthopyroxene) for ^{57}Fe Mössbauer spectroscopy.

Transmission ^{57}Fe Mössbauer spectra of sample powders pressed between two sheets of Fe-free Al foil, or held in Teflon discs, were recorded on a triangular velocity, constant acceleration spectrometer with an ~50 mCi ^{57}Co in Rh source. Phlogopite samples were mixed with sugar in an attempt to obviate preferred orientation effects. All mineral spectra were collected at room temperature but spectra for garnets were also measured at 80 K using a variable temperature cryostat, as the recoil-free fractions of Fe^{2+} and Fe^{3+} in different sites of the garnet structure are temperature dependent (Amthauer *et al.*, 1976). The $Fe^{3+}/\Sigma Fe$ determined for the garnets at 80 K was not extrapolated or corrected to lower temperatures.

Mirror image spectra were recorded over 512 channels with a velocity range of ±5 mm/s and calibrated against Fe metal foil at room temperature. The spectra were fitted using PC-MOS software (CMTE Elektronik, D-85521 Riemerling, Germany) which folds the spectrum and fits the resultant absorption envelope.

Absorber concentrations varied between 2 and 5 mg Fe/cm^2 depending on the amount of clean

Table 1: Sample descriptions[1]

Sample	Description	Locality/Ref.[2]
Southeastern Australia		
84-402	spinel lherzolite, equigranular	Porndon[3]
85-168	spinel lherzolite, granuloblastic tabular	Leura[3]
84-413	phlogopite wehrlite, secondary recrystallized	Noorat[3]
84-438	phlogopite wehrlite, porphyroclastic	Shadwell[3]
BM134	amphibole–spinel lherzolite, porphyroclastic	Bullenmeri[3]
2905	spinel lherzolite, protogranular tabular	Noorat[3]
Tanzania		
89-661	garnet lherzolite, coarse	Lashaine[4]
89-669	wehrlite, protogranular	Lashaine[4]
89-680	garnet harzburgite, coarse	Lashaine[4]
89-719	garnet harzburgite, coarse	Lashaine[4]
89-772	dunite, protogranular	Olmani[4]
89-777	wehrlite, protogranular	Olmani[4]
89-773	harzburgite, protogranular	Olmani[4]
Southern Africa		
BD1140	garnet lherzolite, coarse, low *T*	Bultfontein[5]
BD1150	garnet lherzolite, coarse, low *T*	Bultfontein[5]
BD1201	garnet lherzolite, coarse, low *T*	Wesselton[5]
BD1354	garnet websterite, coarse, low *T*	Matsoku[5]
F865	garnet harzburgite, diamond-bearing, coarse, low *T*	Finsch[6]
F556	garnet harzburgite, diamond-bearing, coarse, low *T*	Finsch[6]
FRB1350	spinel-garnet lherzolite, graphite-bearing, coarse, low *T*	Premier[7]
PHN5267	garnet lherzolite, sheared, high *T*	Premier[8]
PHN5273	garnet harzburgite, coarse, low *T*	Premier[9]
FRB921	garnet websterite, coarse, low *T*	Premier[9]
FRB909	garnet lherzolite, sheared, high *T*	Premier[9]
PHN5239	garnet lherzolite, sheared, high *T*	Premier[9]
Siberia		
UV417/89	garnet lherzolite, coarse, low *T*	Udachnaya[10]
UV61/91	garnet lherzolite, sheared, high *T*	Udachnaya[10]
UV382/86	garnet dunite	Udachnaya[10]
UV465/86	garnet dunite, diamond-bearing	Udachnaya[10]
UV177/89	garnet dunite, diamond-bearing	Udachnaya[10]
UV251/86	garnet dunite	Udachnaya[10]
Norway		
U95	garnet pyroxenite	Ugelvik[11]
U539	garnet pyroxenite	Raudhaugene[11]
Morocco		
GP147	garnet pyroxenite	Beni Boussera[12]
GP87B	garnet pyroxenite	Beni Boussera[12]

[1]Texture classification after Boyd & Mertzman (1987) for garnet-bearing assemblages. [2]Reports of the details of petrography, sample sizes and analytical conditions are given in these references. [3]McDonough & McCulloch (1987) and W. F. McDonough (unpublished, 1993). [4]Rudnick *et al.* (1992, 1993). [5]Carswell & Dawson (1970). [6]Shee *et al.* (1982), Viljoen *et al.* (1992). [7]Pearson *et al.* (1994). [8]Luth *et al.* (1990). [9]F. R. Boyd & D. G. Pearson (unpublished). [10]Pearson *et al.* (1995). [11]Jamtveit *et al.* (1991). [12]Pearson *et al.* (1993).

*Table 2: Compositional data**

Sample	Phase	SiO_2	MgO	Fe_2O_3	FeO	CaO	Al_2O_3	TiO_2	Na_2O	Cr_2O_3	K_2O	Total
SE Australia												
84-402	Ol	40·6	49·8	—	8·9	—	—	—	—	—	—	99·3
	Opx	55·5	33·6	0·37	5·24	0·79	2·5	—	—	0·67	—	98·7
	Cpx	52·5	16·2	0·5	2·05	20·2	3·8	0·28	1·3	1·49	—	98·3
	Sp	—	16·4	3·06	11·7	—	31·2	—	—	38·2	—	100·6
	WR	44·1	43·3	0·17	7·8	0·85	1·2	0·05	0·07	0·82	—	98·4
85-168	Ol	40·7	47·9	—	11·1	—	—	—	—	—	—	99·7
	Opx	55·5	32·6	0·45	6·4	0·68	3·4	—	—	0·65	—	99·7
	Cpx	52·0	16·4	0·75	2·9	18·3	6·6	0·59	1·13	1·27	—	99·9
	Sp	—	17·2	3·72	11·8	—	38·0	—	—	28·7	—	99·4
	WR	44·0	41·5	0·19	10·4	1·12	1·47	0·12	0·1	0·46	—	99·4
84-413	Ol	40·6	47·9	—	11·4	—	—	—	—	—	—	99·9
	Opx	57·9	34·1	*0·54*	6·52	0·43	0·45	—	—	0·25	—	100·2
	Cpx	54·3	15·9	0·48	2·29	20·9	2·74	0·34	1·79	0·87	—	99·6
	Phl	39·0	21·5	1·68	2·69	0·09	14·4	4·59	0·77	0·82	9·02	94·6
	WR	44·1	35·3	*0·41*	10·7	2·6	2·9	0·83	0·39	0·38	—	97·6
84-438	Ol	40·5	47 8	—	11·0	—	—	—	—	—	—	99·3
	Cpx	48·7	14·3	0·21	1·92	22·7	7·53	1·23	0·72	2·08	—	99·2
	Phl	38·9	22·3	3·36	0·96	0·09	16·2	2·48	0·55	1·17	9·4	95·4
	WR	42·4	38·7	0·42	8·8	3·71	2·54	0·37	0·44	0·33	—	97·7
BM-134	Ol	40·7	48·9	—	9·9	—	—	—	—	—	—	99·5
	Opx	56·6	34·4	0·35	5·9	0·24	1·8	—	—	0·28	—	99·6
	Cpx	54·7	15·3	0·39	1·86	19·6	4·28	—	2·33	1·54	—	100·0
	Sp	—	15·5	ND	15·4	—	33·0	—	—	35·2	—	99·1
	Amp	41·5	16·9	1·19	2·41	9·4	12·4	0·36	3·89	2·25	0·32	90·6
	WR	43·1	44·4	0·13	8·8	1·22	1·25	0·04	0·32	0·35	—	99·6
2905	Ol	41·1	49·0	—	9·8	—	—	—	—	—	—	99·9
	Opx	56·0	34·0	0·42	5·9	0·55	4·18	—	—	0·18	—	101·2
	Cpx	52·4	15·3	0·5	2·35	20·3	6·18	0·39	1·57	0·89	—	99·9
	Sp	—	20·3	1·79	9·1	—	57·4	—	—	11·5	—	100·1
	WR	45·1	39·8	0·19	7·5	2·84	3·13	0·11	0·24	0·44	—	99·3
Tanzania												
89-661	Ol	41·2	51·6	—	6·6	—	—	—	—	—	—	99·4
	Opx	57·2	35·5	0·38	3·94	0·44	1·59	0·11	0·14	0·51	—	99·8
	Cpx	54·3	15·7	0·67	1·33	18·6	3·75	0·35	2·59	2·61	—	99·9
	Sp	—	16·9	4·16	9·6	—	17·3	1·4	—	50·5	—	99·9
	WR	42·3	48·0	0·07	6·8	0·94	0·7	0·08	—	0·23	—	99·5
89-669	Ol	40·1	47·9	—	11·4	—	—	—	—	—	—	99·4
	Opx	56·9	33·5	0·58	6·92	0·59	0·53	0·17	0·16	0·45	—	99·8
	Cpx	54·1	16·4	*1·03*	2·51	20·0	1·25	0·42	1·75	2·45	—	99·9
	WR	40·8	43·7	*0·09*	9·5	1·75	0·55	0·1	0·2	—	—	97·0

Table 2: continued

Sample	Phase	SiO_2	MgO	Fe_2O_3	FeO	CaO	Al_2O_3	TiO_2	Na_2O	Cr_2O_3	K_2O	Total
89-772	Ol	40·0	47·3	—	11·9	—	—	—	—	—	—	99·2
	Cpx	54·5	16·3	1·14	2·78	20·8	1·36	0·21	1·35	1·46	—	99·9
	WR	40·6	46·1	0·04	12·5	0·66	0·11	0·02	0·05	0·14	—	100·2
89-680	Ol	41·0	51·6	—	6·94	—	—	—	—	—	99·5	
	Opx	57·2	35·7	0·44	4·01	0·4	1·57	0·04	0·09	0·45	—	99·9
	Cpx	52·9	17·0	0 91	1·45	19·5	4·79	0·16	1·57	1·62	—	99·9
	Sp	—	15·7	3·22	11·6	—	21·6	0·44	—	47·0	—	99·6
	Gtt	42·0	20·5	ND	6·6	5·26	21·2	—	—	4·15	—	99·7
	WR	44·2	45·9	0·15	6·61	0·81	1·22	0·03	—	0·30	—	99·5
89-719	Ol	41·2	51·0	—	7·1	—	—	—	—	—	—	99·3
	Opx	57·3	36·2	0·42	3·94	0·52	0·98	0·04	0·13	0·37	—	99·9
	Cpx	55·1	17·3	0·66	1·46	19·2	2·42	0·11	1·87	1·78	—	99·9
	Gt	41·4	22·2	0·31	5·62	4·84	21·8	0·04	—	3·53	—	99·7
	WR	43·3	43·4	0·07	6·82	0·55	1·09	0·02	—	0·18	—	100·0
89-777	Ol	41·6	52·1	—	5·75	—	—	—	—	—	—	99·5
	Opx	58·5	36·9	—	3·76	0·27	0·20	0·04	0·09	0·14	—	99·9
	Cpx	55·6	17·3	0·51	1·71	19·4	0·78	0·1	1·83	2·7	—	99·9
	Sp	—	16·4	3·60	9·21	—	6·03	0·63	—	64·01	—	99·9
	WR	41·3	48·2	0·08	8·53	1·36	0·17	0·05	—	0·24	—	100·0
89-773	Ol	41·3	51·9	—	6·34	—	—	—	—	—	—	99·5
	Opx	57·6	36·5	0·26	3·79	0·24	1·08	—	—	0·31	—	99·8
	Sp	—	16·0	4·54	10·01	—	21·4	—	—	48·1	—	100·1
	WR	44·1	49·1	0·09	5 97	0·11	0·39	0 01	—	0·25	—	100·0
Southern Africa												
BD 1140	Ol	41·8	49·9	—	7·93	—	—	—	—	—	—	99·6
	Opx	57·8	35·1	0·49	4·46	0·66	0·77	0·06	0·09	0·2	—	99·6
	Cpx	54·8	15·8	0·85	1·55	20·3	2·59	0·16	2·01	1·63	—	99·7
	Gt	41·7	20·9	0·46	7 63	4·2	22·3	0·11	—	1·73	—	99·0
	WR	45·0	41·8	0·18	7·28	1·75	2·58	0·17	0·21	0·34	—	99·2
BD 1150	Ol	41·5	49·3	—	9·43	—	—	—	—	—	—	100·2
	Opx	56·9	35·2	0·63	5·08	0·75	0·72	0·07	0·1	0·2	—	99·7
	Cpx	54·3	16·2	1·03	1·97	19·7	2·62	0·18	1·74	1·74	—	99·5
	Gt	41·6	19·9	0·81	8·09	4·54	21·3	0·02	—	2·64	—	98·9
	WR	46·7	37·6	0·39	7·1	3·49	3·05	0·11	0·4	0·52	—	99·1
BD 1201	Ol	42·1	50·7	—	8·2	—	—	—	—	—	—	101·0
	Opx	57·5	35·3	0·67	5·4	0·34	0·77	0·05	0·07	0·22	—	100·3
	Cpx	54·5	15·9	1·11	1·43	19·6	2·68	0·2	2·32	2·05	—	99·8
	Gt	41·8	20·2	0·29	7·6	4·78	21·7	0·18	—	2·66	—	99·2
	WR	46·7	42·2	0·23	6·8	1·33	1·52	0·07	0·12	0·34	—	99·2

(continued on next page)

Table 2: continued

Sample	Phase	SiO_2	MgO	Fe_2O_3	FeO	CaO	Al_2O_3	TiO_2	Na_2O	Cr_2O_3	K_2O	Total
BD 1354	Ol	40·4	44·2	—	16·5	—	—	—	—	—	—	101·1
	Opx	55·8	31·4	0·64	9·06	1·27	0·77	0·15	0·17	0·19	—	99·5
	Cpx	54·4	16·0	1·55	3·98	17·8	2·46	0·26	1·84	1·22	—	99·5
	Gt	40·9	17·4	1·4	11·6	5·08	19·1	0·52	—	3·97	—	99·9
	WR	47·9	29·3	0·77	11·2	4·38	4·85	0·2	0·44	0·85	—	99·1
PHN 5239	Ol	40·8	50·1	—	8·26	—	—	—	—	—	—	99·2
	Opx	56·4	34·1	0·37	4·47	1·23	0·96	0·29	0·31	0·43	—	98·6
	Cpx	54·0	19·9	0·82	2·76	15·0	2·22	0·42	1·81	1·44	—	98·4
	Gt	41·6	21·5	0·81	6·0	4·95	18·7	1·26	0·1	4·54	—	99·5
	WR	45·6	44·2	0·17	7·22	0·9	1·41	0·2	0·08	0·44	—	100·1
PHN 5273	Ol	41·1	51·1	—	7·68	—	—	—	—	—	—	99·9
	Opx	56·7	35·3	ND	5·5	1·03	0·84	0·05	0·17	0·37	—	100·0
	Cpx	53·5	19·5	ND	2·03	19·2	1·66	0 88	0·89	0·90	—	98·6
	Gt	41·7	21·5	0·71	5·4	5·21	19·2	0·40	—	5·35	—	99·5
	WR	47·4	43·2	ND	6·52	1·11	1·25	0·15	0·08	0·32	—	99·9
FRB 909	Ol	41·1	50·0	—	8·9	—	—	—	—	—	—	100·0
	Opx	56·9	34·8	*0·43*	5·17	1·43	0·97	—	0·24	0·37	—	100·3
	Cpx	54·6	20·7	0·72	2·95	15·9	2·02	0·10	1·42	1·04	—	99·5
	Gt	42·1	22·1	0·88	6·1	4·73	20·2	0·38	—	4·00	—	100·5
	WR	47·01	42·1	*0·21*	8·1	1·63	0·83	0·05	0·12	0·26	—	100·1
FRB 921	Ol	41·0	51·7	—	7·82	—	—	—	—	—	—	100·5
	Opx	57·5	36·2	*0·38*	4·53	0·42	1·05	—	0·12	0·21	—	100·4
	Cpx	54·1	17·0	0·75	1·82	19·7	2·94	0·22	1·99	1·24	—	99·8
	Gt	41·8	21·6	0·35	6·81	4·58	22·31	—	—	2·15	—	99·6
	WR	49·6	35·7	*0·30*	6·14	3·01	4·98	0·04	0·16	0·59	—	100·2
PHN 5267	Ol	41·0	51·2	—	8·74	0·09	0·04	—	—	0·05	—	101·1
	Opx	56·4	35·0	0·44	4·53	1·38	0·91	—	0·16	0·24	—	99·1
	Cpx	56·8	21·5	0·48	2·89	16·8	1·35	—	0·75	0·57	—	101·1
	Gt	42·3	22·3	0·85	5·63	4·93	20·5	0·03	0·02	3·54	—	100·1
	WR	45·2	43·0	0·20	7·51	2·01	1·87	0·03	0·13	0·41	—	100·2
F865	Ol	41·3	50·7	—	6·92	0·03	0·05	0·04	—	0·06	—	99·1
	Opx	58·5	35·5	*0·23*	3·91	0·55	0·49	0·04	0·11	0·30	—	99·6
	Gt	42·5	20·9	0·49	5·57	4·91	19·1	0·21	0·05	5·58	—	99·3
	WR	46·3	44·7	*0·09*	6·83	0·56	1·24	0·05	0·07	0·42	—	100·1
F556	Ol	40·9	50·4	—	8·82	—	—	—	—	—	—	100·1
	Opx	57·5	35·6	*0·27*	4·66	0·77	0·48	—	—	0·23	—	99·5
	Gt	41·3	19·4	0·57	6·65	6·45	17·0	0·16	—	7·44	—	99·0
	WR	48·3	40·7	*0·16*	9·21	0·96	0·61	0·02	0·04	0·24	—	100·1

Table 2: continued

Sample	Phase	SiO_2	MgO	Fe_2O_3	FeO	CaO	Al_2O_3	TiO_2	Na_2O	Cr_2O_3	K_2O	Total
FRB 1350	Ol	41·0	51·7	—	8·3	—	—	—	—	—	—	101·0
	Opx	58·0	36·5	0·35	4·89	0·27	1·13	0·03	—	0·22	—	101·3
	Cpx	54·9	17·3	0·23	1·5	22·9	2·04	0·03	1·23	0·90	—	101·0
	Gt	42·0	20·1	0·31	7·95	5·43	22·1	0·03	—	2·07	—	100·0
	Sp	—	13·4	*2·78*	14·8	—	19·3	0·10	—	49·4	—	99·7
	WR	46·5	42·6	*0·14*	6·84	1·43	1·68	0·01	0·08	0·37	—	99·5
Siberia												
UV 417/89	Ol	40·5	50·8	—	8·81	—	—	—	—	—	—	100·1
	Opx	57·7	36·7	*0·42*	5·03	0·32	0·47	0·09	0·05	0·09	—	100·9
	Cpx	55·0	16·5	0·61	1·73	20·9	2·71	0·25	2·12	0·75	—	100·6
	Gt	41·8	21·3	0·46	8·54	4·38	22 6	0·23	0·04	1·34	—	100·7
	WR	44·7	39·2	*0·21*	8·31	2·93	3·68	0·19	0·14	0·34	—	99·5
UV 61/91	Ol	40·8	51·2	—	8·02	—	—	—	—	—	—	100·0
	Opx	57·6	36·2	*0·38*	4·59	0·73	0·44	0·07	0·11	0·15	—	100·2
	Cpx	55·4	19·2	0·53	2·16	20·2	0·91	0·16	1·03	0·88	—	100·5
	Gt	41·8	19·7	0·85	6·47	6·28	17·5	0·27	—	6·27	—	99·1
	WR	44·6	44·6	*0·14*	7·33	1·68	0·74	0·11	0·10	0·38	—	99·5
UV 382/86	Ol	41·2	51·9	—	6·84	0·03	—	—	—	—	—	99·9
	Gt	41·7	23·7	0·50	7·12	1·65	15·9	0·08	—	8·74	—	99·4
UV 465/86	Ol	41·1	51·7	—	7·33	—	—	—	—	—	—	100·1
	Gt	42·1	22·2	0·42[m]	6·95	3·33	19·6	0·03	—	5·37	—	100·0
UV 177/89	Ol	40·9	51·9	—	7·17	—	—	—	—	—	—	99·9
	Gt	42·4	23·2	0·36	7·14	2·03	20·4	0·03	—	4·54	—	100·1
UV 251/86	Ol	40·9	50·9	—	7·40	—	—	—	—	—	—	99·2
	Opx	58·3	37·1	—	4·40	0·18	0·31	—	—	0·15	—	100·4
	Gt	41·6	22·9	0·44[m]	7·40	2·24	18·7	—	—	6·24	—	99·5
Norway												
U95	Opx	58·6	35·6	NP	4·70	0·13	0·82	—	—	0·21	—	100·0
	Cpx	55·0	15·4	NP	1·26	20·6	2·69	—	2·22	2·40	—	99·6
	Gt	41·6	20·2	NP	8·64	4·61	21·3	—	—	3·52	—	99·9
U539	Ol	39·8	44·1	—	16·50	—	—	—	—	—	—	100·4
	Opx	56·6	31·50	NP	10·10	0·21	0·55	—	—	0·14	—	99·1
	Cpx	54·8	16·90	NP	2·42	24·0	0·52	0·05	0·35	0·42	—	99·5
	Gt	40·2	14·3	NP	14·80	6·27	20·4	0·05	—	3·17	—	99·2
Morocco												
GP147	Gt	40·5	14·48	0·40	16·54	4·69	22·2	0·4	—	0·22	—	99·4
GP87B	Gt	42·0	18·67	0·84	10·66	5·22	22·99	0·11	—	0·50	—	101·0

*Not all minor elements are quoted in some analyses. Original analyses and description of analytical conditions appear in references to each sample listed in Table 1. Whole-rock analyses were not determined for all samples. Values for Fe_2O_3 in italics were estimated using partitioning systematics discussed in the text.

†This phase is present in thin section but replaced partly by spinel.

Ol, olivine; Opx, orthopyroxene; Cpx, clinopyroxene; Sp, spinel; Gt, garnet; Amp, amphibole; Phl, phlogopite; WR, whole rock. [m]Maximum Fe_2O_3 value, using $Fe^{3+}/\Sigma Fe$ determined at room temperature. ND, not determined owing to lack of ^{57}Fe Mössbauer data for one or more phases. NP, not detected in ^{57}Fe Mössbauer spectra.

sample available. The $Fe^{3+}/\Sigma Fe$ ratios derived are insensitive to absorber concentrations within this range (Luth & Canil, 1993). One garnet sample (PHN5267) was measured as a function of absorber thickness at 298 K and its $Fe^{3+}/\Sigma Fe$ was found to be constant over the range 2–5 mg Fe/cm^2. Hyperfine parameters for all samples are listed in Table 3 and descriptions of the fitting models used are given in the Appendix. Extended discussions of the validity and sensitivity of the $Fe^{3+}/\Sigma Fe$ determined for olivines, pyroxenes, spinels and garnets to different spectral fitting procedures have been given by Dyar *et al.* (1989), Luth & Canil (1993), Wood & Virgo (1989) and Luth *et al.* (1990), respectively, and will not be repeated here.

RESULTS

The distribution of Fe^{3+} in the spinel peridotite facies

Overview

In the following discussion, we make use of both our new data, and data in the literature (Dyar *et al.*, 1989, 1992; McGuire *et al.*, 1991; Luth & Canil, 1993) to interpret the crystal chemical controls on the distribution of Fe^{3+} amongst upper-mantle minerals.

In spinel lherzolites, $Fe^{3+}/\Sigma Fe$ varies from 0·04 to 0·09 in orthopyroxene, and from 0·12 to 0·36 in clinopyroxene. The spinels coexisting with these pyroxenes have $Fe^{3+}/\Sigma Fe$ from 0·15 to 0·34. A larger database of reliable $Fe^{3+}/\Sigma Fe$ determinations on mantle spinels (e.g. Wood & Virgo, 1989; Bryndzia & Wood, 1990; Canil *et al.*, 1990; Woodland *et al.*, 1992; Ionov & Wood, 1993) confirms that nearly all primary mantle spinels from spinel lherzolite and spinel harzburgite xenoliths fall within the range covered by samples in this study, but also reveals that abyssal peridotites and orogenic massif peridotite spinels generally have lower $Fe^{3+}/\Sigma Fe$, mostly in the range 0·05–0·15 (Bryndzia & Wood, 1990; Woodland *et al.*, 1992).

The details of the distribution of Fe^{3+} between different phases of mantle peridotites are complex. The amount of Fe^{3+} in a particular phase is expected to depend on the whole-rock Fe^{3+}, the modal abundances of the Fe^{3+}-containing phases, their chemical composition (especially important for coupled substitutions) and the chemistry of other coexisting phases, as well as the thermodynamic variables of pressure and temperature. These factors are not mutually independent, and cannot be treated in isolation. Nevertheless, we can use the empirical partitioning data to identify which factors are of most importance.

Fe^{3+} in pyroxenes

There is a good correlation between the amount of Fe^{3+} in orthopyroxene with that in coexisting clinopyroxene from spinel lherzolites (Fig. 1). The scatter is not much greater than that expected from the uncertainties in the $Fe^{3+}/\Sigma Fe$ determinations. As both orthopyroxene and clinopyroxene share the same stoichiometry in terms of cation-to-oxygen ratio, they can be described using the same thermodynamic components. Thus, the partitioning reactions controlling the distribution of elements between coexisting pyroxenes are not directly affected by the nature of the other coexisting phases. This eliminates one possible cause of scatter in such partitioning diagrams.

The empirical distribution coefficient $D_{Fe^{3+}}^{opx/cpx}$ is $0{\cdot}62 \pm 0{\cdot}04$. For comparison, the equivalent empirical distribution coefficients $D_{Ti}^{opx/cpx}$ and $D_{Na}^{opx/cpx}$ for two other minor elements, Ti and Na, which show a roughly similar degree of moderately incompatible behaviour during mantle melting, are plotted in Fig. 2. We find $D_{Ti}^{opx/cpx} = 0{\cdot}24 \pm 0{\cdot}02$, with similar scatter to that for $D_{Fe^{3+}}^{opx/cpx}$, whereas $D_{Na}^{opx/cpx} = 0{\cdot}067 \pm 0{\cdot}004$, but the scatter appears somewhat greater (perhaps indicating that the partitioning of Na between orthopyroxene and clinopyroxene is also influenced by temperature and/or pressure). The important point is that $D_{Fe^{3+}}^{opx/cpx}$ is much closer to unity than is $D_{Ti}^{opx/cpx}$ or $D_{Na}^{opx/cpx}$.

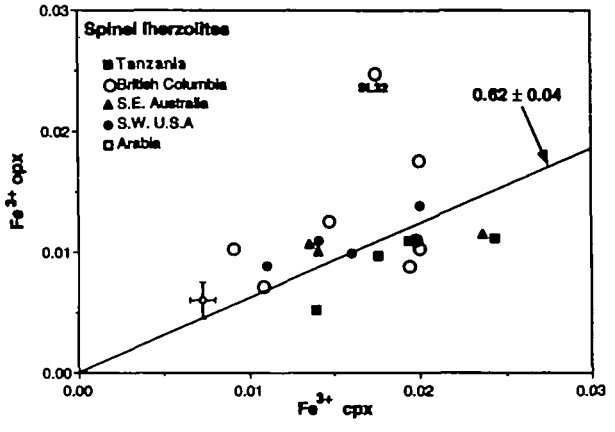

Fig. 1. Partitioning of atomic Fe^{3+} (based on four cation stoichiometry) between coexisting clino- and orthopyroxenes in spinel lherzolites. Data sources are: SW USA and Arabia, Dyar *et al.* (1989, 1992) and McGuire *et al.* (1991). All other data are from this study and Luth & Canil (1993). The value of $D^{Fe^{3+}}$ was obtained by linear regression of the data using a single-parameter model (i.e. without a constant, which constrains the regression to pass through the origin). The quoted uncertainty is the standard error of the estimate from this model.

Table 3: Hyperfine parameters (all given relative to Fe metal foil at room temperature)

Sample	Fe^{2+} (I)			Fe^{2+} (II)				Fe^{2+} (III)				Fe^{3+}				χ^2
	IS	QS	FWHH	IS	QS	FWHH	Area	IS	QS	FWHH	Area	IS	QS	FWHH	Area	
SE Australia																
85-168																
Opx	1·17	2·13	0·29	1·22	2·43	0·3	0·146	1·06	2·09	0·27	0·326	0·32	0·88	0·45	0·06	960
Cpx	1·13	2·04	0·46	1·15	2·56	0·41	0·159	—	—	—	—	0·35	0·58	0·66	0·2	481
Sp	0·94	1·85	0·46	1·17	0·9	0·52	0·403	—	—	—	—	0·28	0·74	0·33	0·23	781
Ol	1·11	2·79	0·26	1·11	2·99	0·22	0·392	—	—	—	—	—	—	—	—	282
84-402																
Opx	1·06	2·15	0·29	1·23	2·43	0·19	0·063	1·08	2·09	0·33	0·38	0·29	0·86	0·53	0·07	919
Cpx	1·13	1·96	0·45	1·07	2·31	0·42	0·252	—	—	—	—	0·26	0·72	0·66	0·18	299
Sp	0·83	1·76	0·49	0·9	1·08	0·51	0·382	—	—	—	—	0·28	0·69	0·3	0·19	1354
2905																
Opx	1·18	2·15	0·31	1·23	2·44	0·34	0·14	1·04	2·1	0·36	0·322	0·31	0·89	0·5	0·06	586
Cpx	1·13	1·96	0·45	1·2	2·32	0·43	0·328	—	—	—	—	0·26	0·82	0·61	0·16	404
Sp	0·89	1·87	0·41	0·88	1·21	0·54	0·515	—	—	—	—	0·24	0·74	0·3	0·15	428
BM134																
Ol	1·12	2·88	0·25	1·14	3·07	0·25	0·521	—	—	—	—	—	—	—	—	507
Opx	1·12	2·06	0·28	1·17	2·47	0·34	0·151	1·04	1·96	0·29	0·21	0·31	0 97	0·72	0·05	376
Cpx	1·14	2·04	0·45	1·16	2·61	0·49	0·254	—	—	—	—	0·51	0·39	0·51	0·16	356
Amp-3	1·1	2·42	0·33	1·12	2·74	0·3	0·261	1·09	1·86	0·35	0·205	0·35	0·78	0·75	0·31	330
Amp-2	1·1	1·91	0·39	1·12	2·63	0·37	0·449	—	—	—	—	0·33	0·81	0·69	0·3	445
84-438																
Ol	1·12	2·88	0·26	1·14	3·07	0·25	0·48	—	—	—	—	—	—	—	—	297
Cpx	1·15	1·97	0·41	1·18	2·31	0·52	0·26	—	—	—	—	0·29	0·8	0·65	0·19	310
Phl*	1·09	3·01	0·39	1·06	2·83	0·38	0·086	1·1	2·26	0·31	0·094	0·41	1·21	0·62	0·76	515
84-413																
Ol	1·08	2·76	0·25	1·1	2·95	0·22	0·404	—	—	—	—	—	—	—	—	322
Cpx	1·13	2·06	0·47	1·14	2·82	0·34	0·116	—	—	—	—	0·37	0·4	0·56	0·16	323
Phl	1·06	2·39	0·35	1·03	1·98	0·32	0·162	—	—	—	—	0·36	0·99	0·58	0·36	481
Tanzania																
89-772																
Cpx	1·16	1·97	0·45	1·36	2·4	0·3	0·099	—	—	—	—	0·25	0·85	0·61	0·27	330
Ol	1·14	2·89	0·26	1·16	3·09	0·24	0·464	—	—	—	—	—	—	—	—	586
89-669																
Opx	1·16	2·13	0·25	1·2	2·55	0·45	0·182	1·07	2·06	0·28	0·257	0·36	0·54	0·58	0·07	865
89-661																
Opx	1·25	2·29	0·32	1·3	2·51	0·35	0·194	1·11	2·3	0·39	0·188	0·43	0·94	0·53	0·08	297
Cpx	1·22	2·18	0·46	1·23	2·74	0·53	0·206	—	—	—	—	0·43	0·74	0·74	0·3	269
Sp	1·01	1·77	0·56	0·97	1·07	0·55	0·377	—	—	—	—	0·34	0·62	0·34	0·28	264
Ol	1·09	2·81	0·25	1·11	2·97	0·22	0·368	—	—	—	—	—	—	—	—	251

(continued on next page)

Table 3: continued

Sample	Fe^{2+} (I)			Fe^{2+} (II)				Fe^{2+} (III)				Fe^{3+}				χ^2
	IS	QS	FWHH	IS	QS	FWHH	Area	IS	QS	FWHH	Area	IS	QS	FWHH	Area	
89-680																
Opx	1·24	2·31	0·29	1·31	2·62	0·32	0·105	1·11	2·17	0·34	0·116	0·33	0·66	0·47	0·09	351
Cpx	1·13	1·9	0·41	1·18	2·26	0·39	0·322	—	—	—	—	0·3	0·61	0·68	0·36	259
Sp	0·92	1·61	0·53	0·9	0·91	0·5	0·315	—	—	—	—	0·31	0·59	0·41	0·28	440
89-719																
Opx	1·15	2·09	0·29	1·16	2·42	0·28	0·123	1·01	2·06	0·29	0·188	0·2	0·14	0·43	0·09	305
Cpx	1·14	2·04	0·45	1·18	2·32	0·14	0·09	—	—	—	—	0·22	0·52	0·68	0·31	267
Gt-298	1·28	3·55	0·36	—	—	0·28	—	—	—	—	—	0·27	0·27	0·59	0·075	338
Gt-80	1·41	3·66	0·42	—	—	0·34	—	—	—	—	—	0·3	0·31	0·41	0·048	535
89-773																
Opx	1·16	2·11	0·39	1·19	2·41	0·27	0·146	1·05	2·04	0·28	0·146	0·39	0·68	0·57	0·05	686
Sp	0·92	1·61	0·54	0·9	0·95	0·45	0·263	—	—	—	—	0·31	0·61	0·35	0·29	579
89-777																
Cpx	1·16	1·98	0·48	1·29	2·45	0·31	0·094	—	—	—	—	0·2	0·76	0·57	0·21	255
Sp	0·91	1·34	0·49	0·89	0·78	0·44	0·389	—	—	—	—	0·34	0·52	0·3	0·26	696
Ol	1·14	2·89	0·27	1·15	3·1	0·25	0·481	—	—	—	—	—	—	—	—	325
South Africa																
BD1140																
Opx	1·15	2·12	0·24	1·18	2·46	0·3	0·176	1·1	2·06	0·26	0·25	0·13	0·13	0·8	0·09	268
Cpx	1·16	2·03	0·45	1·31	2·45	0·34	0·068	—	—	—	—	0·28	0·66	0·66	0·33	269
Gt-298	1·28	3·57	0·33	—	—	0·28	—	—	—	—	—	0·24	0·07	0·82	0·067	415
Gt-80	1·67	4·38	0·44	—	—	0·38	—	—	—	—	—	0·33	0·02	0·76	0·051	635
Ol	1·08	2·75	0·23	1·11	2·92	0·24	—	—	—	—	—	—	—	—	—	312
BD1150																
Opx	1·13	2·03	0·23	1·14	2·32	0·29	0·17	1·06	2·01	0·24	0·397	0·03	0·1	0·59	0·1	297
Cpx	1·16	1·98	0·45	1·27	2·37	0·34	0·124	—	—	—	—	0·27	0·75	0·57	0·32	276
Gt-298	1·29	3·57	0·32	—	—	0·27	—	—	—	—	—	0·25	0·23	0·82	0·084	374
Gt-80	1·31	3·67	0·43	—	—	0·39	—	—	—	—	—	0·26	0·43	0·75	0·083	553
Ol	1·09	2·75	0·25	1·1	2·93	0·24	—	—	—	—	—	—	—	—	—	289
BD1201																
Opx	1·12	2·04	0·22	1·14	2·36	0·29	0·17	1·06	2	0·25	0·31	0·16	0·08	0·93	0·1	264
Cpx	1·15	1·93	0·38	1·21	2·25	0·42	0·272	—	—	—	—	0·26	0·62	0·64	0·41	292
Gt-298	1·29	3·58	0·32	—	—	0·27	—	—	—	—	—	0·31	0·25	0·39	0·048	259
Gt-80	1·42	3·64	0·34	—	—	0·29	—	—	—	—	—	0·39	0·03	0·41	0·033	297
BD1354																
Opx	1·11	2·07	0·23	1·15	2·33	0·32	0·159	1·09	1·92	0·26	0·346	0·31	0·74	0·41	0·06	310
Cpx	1·13	2·01	0·38	1·24	2·22	0·46	0·288	—	—	—	—	0·3	0·65	0·53	0·26	527
Gt-298	1·29	3·58	0·31	—	—	0·27	—	—	—	—	—	0·3	0·29	0·41	0·103	438
Gt-80	1·41	3·62	0·32	—	—	0·3	—	—	—	—	—	0·4	0·25	0·46	0·098	566

Table 3: continued

Sample	Fe^{2+} (I)			Fe^{2+} (II)				Fe^{2+} (III)				Fe^{3+}				χ^2
	IS	QS	FWHH	IS	QS	FWHH	Area	IS	QS	FWHH	Area	IS	QS	FWHH	Area	
PHN5267																
Opx	1·15	2·09	0·22	1·16	2·33	0·38	0·264	1·07	2·02	0·25	0·195	0·27	0	0·65	0·08	271
Cpx	1·09	1·98	0·31	1·05	1·81	0·26	0·24	—	—	—	—	0·24	0·56	0·63	0·13	277
Gt-298	1·29	3·58	0·35	—	—	0·28	—	—	—	—	—	0·32	0·32	0·39	0·159	260
Gt-80	1·44	3·70	0·40	—	—	0·30	—	—	—	—	—	0·46	0·28	0·43	0·121	475
FRB909																
Cpx	1·15	2·09	0·35	1·1	1·89	0·25	0·191	—	—	—	—	0·25	0·24	0·79	0·18	463
Gt-298	1·28	3·56	0·33	—	—	0·27	—	—	—	—	—	0·32	0·28	0·44	0·126	282
Gt-80	1·42	3·64	0·43	—	—	0·35	—	—	—	—	—	0·38	0·28	0·42	0·115	363
PHN5239																
Cpx	1·18	2·12	0·38	1·11	1·97	0·28	0·345	—	—	—	—	0·22	0·49	0·71	0·21	302
Gt-80	1·41	3·64	0·43	—	—	0·35	—	—	—	—	—	0·42	0·29	0·45	0·108	334
Gt-298	1·29	3·55	0·35	—	—	0·29	—	—	—	—	—	0·35	0·33	0·43	0·129	255
PHN5273																
Gt-80	1·43	3·64	0·43	—	—	0·35	—	—	—	—	—	0·41	0·31	0·44	0·119	409
FRB921																
Cpx	1·23	2·19	0·51	1·13	2·02	0·45	0·424	—	—	—	—	0·27	0·67	0·59	0·27	317
Gt-80	1·41	3·64	0·43	—	—	0·36	—	—	—	—	—	0·33	0·33	0·41	0·044	497
Gt-298	1·28	3·56	0·33	—	—	0·28	—	—	—	—	—	0·26	0·39	0·45	0·057	267
F865[c]																
Gt-298	1·29	3·56	0·34	—	—	0·28	—	—	—	—	—	0·28	0·31	0·39	0·102	
Gt-80	1·43	3·64	0·47	—	—	0·38	—	—	—	—	—	0·28	0·29	0·43	0·074	347
F556[c]																
Gt-80	1·31	3·64	0·43	—	—	0·35	—	—	—	—	—	0·39	0·27	0·39	0·072	343
FRB1350[c]																
Opx	1·15	2·14	0·26	1·18	2·78	0·49	0·22	1·11	2·01	0·28	0·21	0·31	0[f]	0·75[f]	0·06	967
Cpx	1·19	2·31	0·47	1·15	1·96	0·39	0·65	—	—	—	—	0·27	0·93	0·47	0·12	276
Gt-298	1·29	3·56	0·33	—	—	0·28	—	—	—	—	—	0·29	0·46	0·41	0·044	829
Siberia																
UV61/91																
Cpx	1·29	2·21	0·37	1·12	2·01	0·32	0·708	—	—	—	—	0·26	0·59	0·65	0·18	284
Gt-298	1·29	3·54	0·34	—	—	0·28	—	—	—	—	—	0·32	0·31	0·38	0·12	258
Gt-80	1·43	3·64	0·47	—	—	0·41	—	—	—	—	—	0·41	0·29	0·45	0·106	399
UV417/89																
Cpx	1·18	2·26	0·51	1·14	1·95	0·38	0·319	—	—	—	—	0·39	0·46	0·62	0·24	276
Gt-298	1·31	3·56	0·33	—	—	0·28	—	—	—	—	—	0·28	0·27	0·51	0·06	286
Gt-80	1·43	3·63	0·43	—	—	0·38	—	—	—	—	—	0·37	0·31	0·45	0·046	487

(continued on next page)

Table 3: continued

Sample	Fe^{2+} (I)			Fe^{2+} (II)				Fe^{2+} (III)				Fe^{3+}				χ^2
	IS	QS	FWHH	IS	QS	FWHH	Area	IS	QS	FWHH	Area	IS	QS	FWHH	Area	
UV382/86																
Gt-298	1·29	3·56	0·34	—	—	0·27	—	—	—	—	—	0·32	0·15	0·46	0·064	320
UV465/86[c]																
Gt-298	1·29	3·57	0·34	—	—	0·27	—	—	—	—	—	0·32	0·27	0·33	0·055	276
UV177/89[c]																
Gt-298	1·29	3·54	0·34	—	—	0·29	—	—	—	—	—	0·32	0·26	0·43	0·051	266
Gt-80	1·42	3·66	0·49	—	—	0·41	—	—	—	—	—	0·36	0·24	0·45	0·045	338
UV251/86																
Gt-298	1·28	3·56	0·34	—	—	0·27	—	—	—	—	—	0·31	0·26	0·41	0·053	236
Norway																
U95																
Opx	1·14	2·09	0·23	1·16	2·26	0·27	0·238	1·05	1·94	0·34	0·144	0·27	0·06	0·71	0·001	1185
Gt-298	1·29	3·58	0·33	—	—	0·28	—	—	—	—	—	0·11	0·19	0·84	0·019	271
U539																
Opx	1·15	2·08	0·25	1·18	2·25	0·32	0·254	1·04	2·04	0·3	0·155	—	—	—	—	2266
Cpx	1·14	2·01	0·32	1·24	2·09	0·57	0·229	—	—	—	—	—	—	—	—	451
Gt-298	1·29	3·57	0·31	—	—	0·28	—	—	—	—	—	—	—	—	—	591
Beni Bousera																
GP147[c]																
Gt-298	1·29	3·55	0·32	—	—	0·29	—	—	—	—	—	0·29	0·29	0·4	0·022	348
GP87B[c]																
Gt-298	1·28	3·55	0·32	—	—	0·29	—	—	—	—	—	0·32	0·33	0·45	0·071	326

*Three doublets were required for Fe^{2+} to obtain convergence.
†This parameter was fixed during fitting to attain convergence.
[c]Coexisting with carbon as either graphite or diamond (see Table 1).
IS, isomer shift; QS, quadrupole splitting; FWHH, full width at half height; Area, fraction of total resonance envelope. Ol, olivine; Opx, orthopyroxene; Cpx, clinopyroxene; Sp, spinel; Gt, garnet; Amp, amphibole; Phl, phlogopite. Amp-2, result using two doublet fit for Fe^{2+}. Amp-3, result using three doublet fit for Fe^{2+}. Gt-80, garnet measured at 80 K. FWHH are for the low-velocity and high-velocity peaks, respectively. Gt-298, garnet measured at room temperature.

Therefore, as important amounts of Fe^{3+}, and not Na or Ti, also occur in mantle spinels, Fe^{3+} is much more homogeneously distributed among the phases than are other moderately incompatible elements.

Unfortunately, the Mössbauer spectra obtained in this study cannot be used to elucidate the actual substitution mechanism of Fe^{3+} in pyroxenes, owing to the difficulty of obtaining unique hyperfine parameters for poorly resolved Fe^{3+} contributions to the resonance envelope in pyroxenes (Dollase, 1975). There is, however, some information from synthetic simple systems which may be coupled to the empirical observations of this study to estimate the probable substitution mechanisms, as the first step in the development of a thermodynamic model for the partitioning of Fe^{3+} in upper-mantle phases.

The possibility of different types of substitutions which are stoichiometrically independent of each other in pyroxenes requires them to be treated as reciprocal solutions (Luth & Canil, 1993), so that

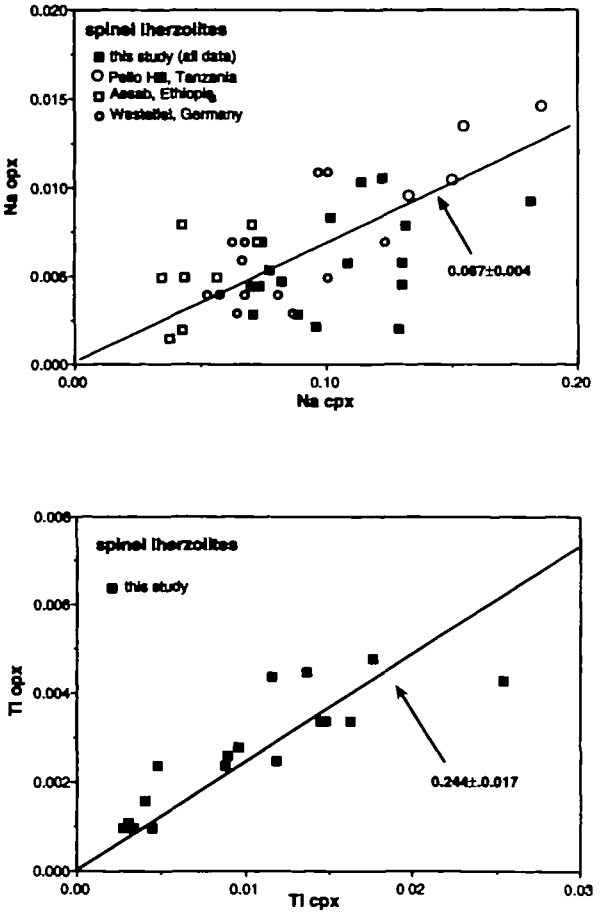

Fig. 2. Covariation of Ti and Na atoms (based on four cation stoichiometry) in coexisting clino- and orthopyroxenes in spinel lherzolites. Data sources are: Pello Hill, Dawson & Smith (1988); Assab, Ottonello *et al.* (1978); Westeifel, Sachtleben & Seck (1981). All other data are from this study and Luth & Canil (1993). The quoted uncertainty is the standard error of the estimate.

within an assumed solution model, all of the possible components need to be considered simultaneously. Given its ionic radius, standard crystal chemical arguments suggest that Fe^{3+} substitutes onto the M1 octahedral site, with charge balance maintained by the coupled substitution of either Al for Si on a tetrahedral site (Annersten *et al.*, 1978), or Na on the M1 site. The Fe^{3+} components in pyroxenes would then be either the acmite component, $NaFe^{3+}Si_2O_6$, or the components $MFe^{3+}AlSiO_6$ where M = Mg, Fe^{2+} and Ca (e.g. $CaFe^{3+}AlSiO_6$, esseneite; Cosca & Peacor, 1987). These components embody coupled substitutions of the type $Na^{(M2)} + Fe^{3+(M1)} = Ca^{(M2)} + Mg^{(M1)}$ and $Fe^{3+(M1)} + Al^{(T)} = Mg^{(M1)} + Si^{(T)}$. The empirical evidence, however, shows no correlation of Fe^{3+} with Al or Na in clinopyroxene (Fig. 3a). This surprising finding is supported by the experimental data of Annersten *et al.* (1978), who studied the substitution of Fe^{3+} into orthopyroxene in the system $MgO–SiO_2–FeO–Fe_2O_3 \pm Al_2O_3$ at 2 kbar and 800–1000°C at very high f_{O_2}, and were able to demonstrate substantial Fe^{3+} contents in Al- (and Na-) free orthopyroxenes, and by Huckenholz *et al.* (1969), who studied the $CaFe_2^{3+}SiO_6$ substitution in diopside and demonstrated the presence of tetrahedral Fe^{3+} by Mössbauer spectroscopy.

Also supporting the lack of influence of the Al-coupled substitution on Fe^{3+} in pyroxenes is the observation that at least one orthopyroxene with a low Al content (sample 89-669) has molar $Al < (Fe^{3+} + Cr)$, which means that its chemical formula must contain tetrahedral Fe^{3+}. Any such pyroxene must have a finite activity of its $MgAl_2SiO_6$ component, implying that Al and Fe^{3+} are to some extent distributed between the M1 octahedral and tetrahedral sites in pyroxenes.

Taken together, these observations suggest that perhaps the appropriate description for Fe^{3+}

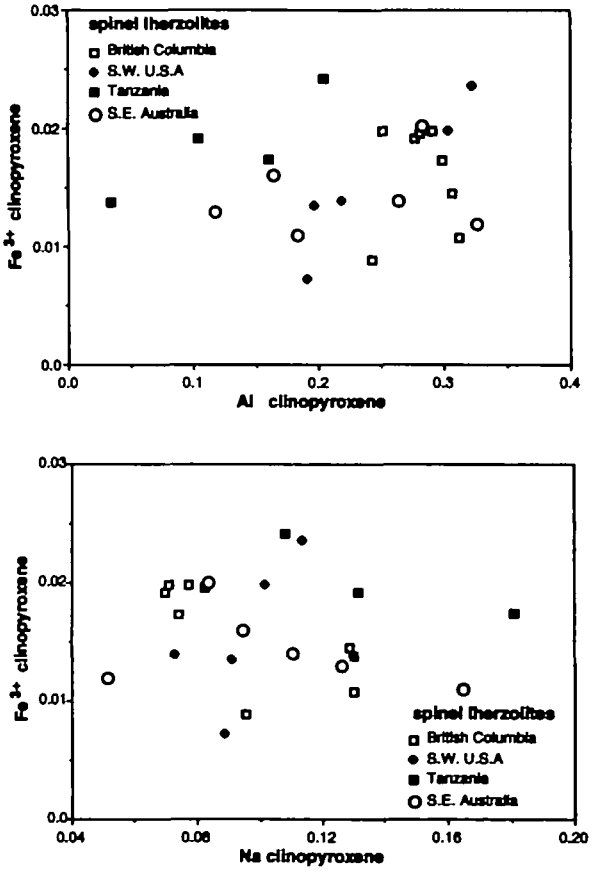

Fig. 3. Covariation of Fe^{3+} (based on four cation stoichiometry) with (a) Al and (b) Na in clinopyroxene. Data sources as in Fig. 2. In neither case is any correlation apparent.

substitutions in pyroxenes should involve the $MFe_2^{3+}SiO_6$ type of component, rather than the Al-coupled $MFe^{3+}AlSiO_6$ components, together with provision for Fe^{3+}–Al ordering between the M1 and tetrahedral sites. This may have considerable significance for the determination of the activity of the $MgAl_2SiO_6$ component in natural Fe^{3+}-bearing orthopyroxenes, and thus on the geobarometry of garnet lherzolites calibrated using Al-in-orthopyroxene (e.g. Brey & Köhler, 1990; Carswell, 1991).

Perhaps equally surprising, Na also does not affect the substitution of Fe^{3+} in pyroxene. The amount of Na in the clinopyroxene of our samples varies by nearly a factor of four, but Fig. 3b shows that no correlation between Na and Fe^{3+} in clinopyroxene exists. The reciprocal reactions between components with and without Na are

$$MAl_2SiO_6 + NaFe^{3+}Si_2O_6 = MFe^{3+}AlSiO_6 + NaAlSi_2O_6 \quad (1)$$

or, if the $MFe_2^{3+}SiO_6$ type of end-member is chosen,

$$MAl_2SiO_6 + 2\ NaFe^{3+}Si_2O_6 = MFe_2^{3+}SiO_6 + 2\ NaAlSi_2O_6. \quad (2)$$

The implication is therefore that the free energy of the reciprocal reactions [(1) or (2)] in clinopyroxene is likely to be small.

The Fe^{3+} content of pyroxenes could potentially be influenced by the Mg/Fe^{2+} ratio of coexisting olivine, through redox reactions of the type

$$\underset{\text{olivine}}{Fe_2SiO_4} + \underset{\text{olivine}}{Mg_2SiO_4} + \underset{\text{clinopyroxene}}{CaMgSi_2O_6} + 0{\cdot}5\ O_2 = \underset{\text{clinopyroxene}}{CaFe_2^{3+}SiO_6} + 1{\cdot}5\ \underset{\text{orthopyroxene}}{Mg_2Si_2O_6}. \quad (3)$$

Reaction (3) demonstrates that a negative correlation between atomic Fe^{3+} in clinopyroxene vs *mg*-number in coexisting olivine would be expected if upper-mantle f_{O_2} were buffered at some constant level. Figure 4 shows that we find no such negative correlation in any of the studied xenolith suites, indicating that upper-mantle f_{O_2} is not externally buffered in such suites. Composite xenoliths, however, studied by McGuire *et al.* (1991) and Dyar *et al.* (1992), each presumably equilibrated at a single T and P, do indeed show the negative correlation expected from equation (3) (Fig. 5). This observation indicates an approach to equilibrium in f_{O_2} over the length scale of the composite xenoliths (centimetres), which might imply the action of a localized fluid operating in the mantle, consistent with other petrographic observations in these xenoliths (McGuire *et al.*, 1991; Dyar *et al.*, 1992).

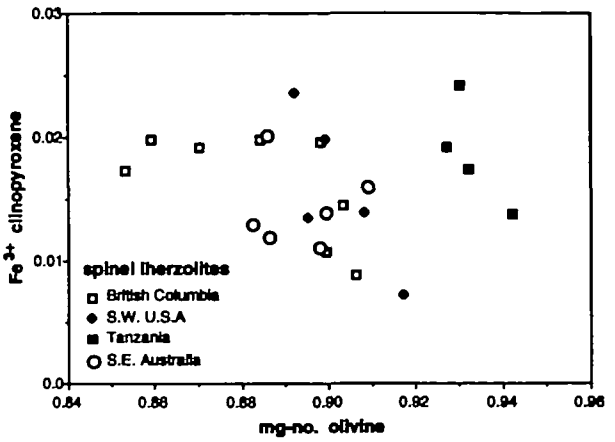

Fig. 4. Covariation of Fe^{3+} in clinopyroxene (based on four cation stoichiometry) and $Mg/(Mg+Fe)$ (*mg*-number) in coexisting olivine from spinel lherzolites. Data sources as in Fig. 2. No correlation is apparent, implying [from reaction (4)] that f_{O_2} is not externally controlled in these xenolith suites on the spatial scale from which they are sampled.

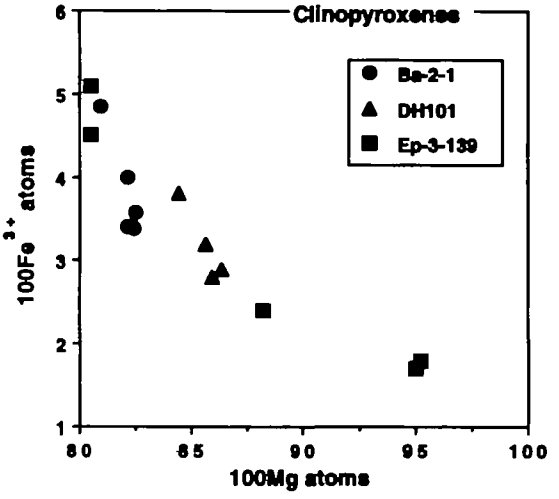

Fig. 5. Plot showing the negative correlation of Fe^{3+} (based on four cation stoichiometry) with $Mg/(Mg+Fe)$ in clinopyroxene from three composite spinel peridotite xenoliths described by McGuire *et al.* (1991) and Dyar *et al.* (1992). In contrast to xenolith suites (see Fig. 4), these composite xenoliths show the negative correlation expected from reaction (4) if f_{O_2} is locally buffered (e.g. by a fluid phase).

There is a positive correlation between the temperature of equilibration of the xenoliths and Fe^{3+} in clinopyroxene (Fig. 6a). This trend may be due directly to the influence of temperature on the intercrystalline partitioning relationships of Fe^{3+} or, indirectly, as a by-product of decreasing Ca in clinopyroxene with increasing temperature, if Ca in clinopyroxene exerts a crystal-chemical control through a large positive free energy for the reciprocal reaction

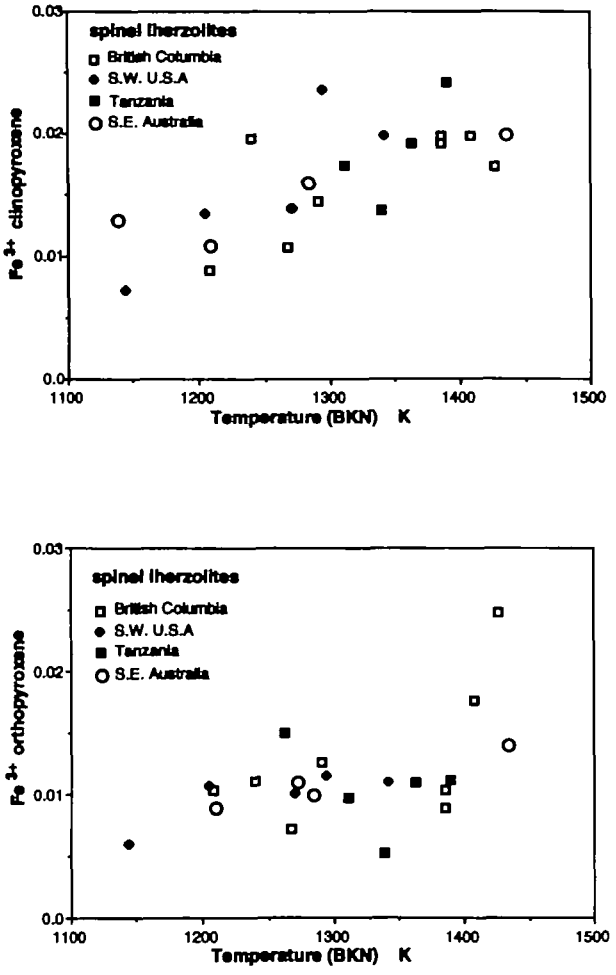

Fig. 6. Variation of Fe^{3+} in coexisting clino- and orthopyroxene with temperature [in Kelvin, calculated using the two-pyroxene method (BKN) of Brey & Köhler (1990)]. Data sources as in Fig. 2.

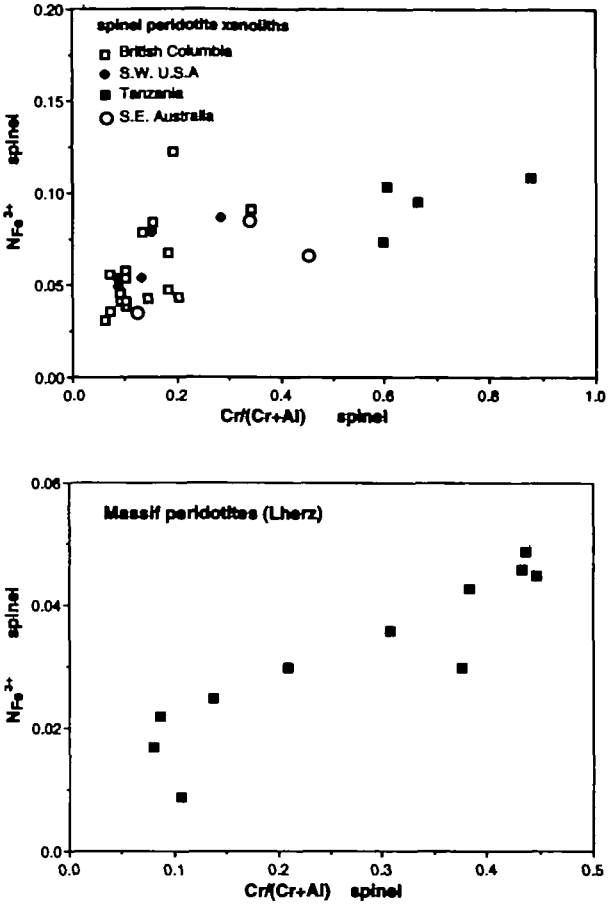

Fig. 7. Variation of Fe^{3+} cations in spinel with Cr/(Cr + Al) in spinel from xenoliths and the Lherz orogenic peridoite massif. Data sources are: xenoliths, as in Fig. 2; massif peridotites, Woodland *et al.* (1992).

$$CaFe_2^{3+}SiO_6 + MgAl_2SiO_6 = MgFe_2^{3+}SiO_6 + CaAl_2SiO_6. \quad (4)$$

There is only a slight indication of any correlation of Fe^{3+} with temperature in orthopyroxene (Fig. 6b), which could be taken to support the latter scenario. Alternatively, any effect in orthopyroxene may be masked by the greater relative uncertainty in the Fe^{3+} determinations.

Fe^{3+} in spinel

Fe^{3+} in spinel is positively correlated with Cr/(Cr + Al), both in xenoliths and in orogenic massif peridotites as at Lherz, France (Fig. 7). This is expected, as the excess free energies of mixing of Fe^{3+}–Cr spinels are lower than those of Fe^{3+}–Al spinels (e.g. O'Neill & Wall, 1987). There are at least three additional factors, however, to complicate this explanation. First, increasing Cr/(Cr + Al) in spinel is positively correlated with increasing degree of depletion in mantle peridotites, and hence with decreasing whole-rock Fe^{3+}. This should act to oppose the crystal-chemical effect. Second, the modal amount of spinel can also be expected to change with degree of depletion. Using the parameterization of melting reactions for spinel lherzolite of Kinzler & Grove (1992) we calculate that ~3% modal spinel in a typical fertile peridotite will decrease to a near-zero value only after ~30% partial melting. Lastly, the modal amount of spinel is also a function of temperature of equilibration, a more or less completely independent variable. Modal pyroxenes will increase at the expense of spinel at higher temperatures approaching the mantle solidus (Green & Ringwood, 1967). For some peridotites, spinel may not be stable on the mantle solidus during partial melting (Walter & Presnall, 1994).

Fe^{2+} is also positively correlated with Cr/(Cr + Al) in spinel, owing to the reciprocal solid solution effect (e.g. Wood & Nicholls, 1977). This phenomenon is well known from its effect on the olivine–spinel Fe^{2+}–Mg exchange equilibria and its calibration as a geothermometer (Irvine, 1965). As the magnitude of this correlation happens to be similar to the influence of Cr/(Cr + Al) on Fe^{3+}, the net result is that the ratio $Fe^{3+}/\Sigma Fe$ shows no correlation with Cr/(Cr + Al), consistent with the experimental data of Ballhaus *et al.* (1991) on orthopyroxene–olivine–spinel assemblages.

As in the pyroxenes, the Fe^{3+} in spinel also increases with increasing equilibration temperature, although the effect is somewhat obscured by the stronger correlation with Cr/(Cr + Al). This correlation becomes more noticeable when the slowly cooled massif peridotites, which contain spinels with lower average $Fe^{3+}/\Sigma Fe$, are compared with xenoliths.

Fe^{3+} in hydrous phases

Large amounts of Fe^{3+} can reside in upper-mantle hydrous phases such as amphibole and phlogopite [Tables 2 and 3, and McGuire *et al.* (1991)]. The amphibole and phlogopite with $Fe^{3+}/\Sigma Fe$ ratios similar to those of coexisting clinopyroxene in samples BM-134 and 84-413 (~0·30–0·35) may represent real equilibrium values. In contrast, phlogopite in sample 84-438, a rock with identical Mg/Fe to 84-413 and BM134, has $Fe^{3+}/\Sigma Fe$ of 0·76. In the latter sample, the Mg/Fe^{2+} of phlogopite should be similar to that in 84-413, as it is controlled by Mg/Fe^{2+} in olivine, which is identical in these two samples (Table 2). Clearly, phlogopite in 84-438 has a much higher Mg/Fe^{2+}, and thus most of the original Fe^{2+} in this phase must have been oxidized at a late stage to Fe^{3+}. This disequilibrium effect was probably caused by dehydroxylation–oxidation of the phlogopite according to the reaction

$$Fe^{2+} + OH^- = Fe^{3+} + O^{2-} + 1/2\ H_2. \qquad (5)$$

The bulk Fe_2O_3 contents of hydrous samples are typically above that expected for unmetasomatized peridotites showing a similar level of major element depletion (Canil *et al.*, 1994). Clearly, if the Fe^{3+} in the hydrous phases is primary, this would argue that Fe^{3+} was added to the bulk assemblage by the hydrous fluid responsible for the metasomatism (McGuire *et al.*, 1991). The fluid could then be identified as being of an unusually oxidized nature. Conversely, if the extra Fe^{3+} in the hydrous phases is secondary, the metasomatic fluid need not necessarily have been oxidizing.

The partitioning of Fe^{3+} between spinel and pyroxenes

The empirical evidence discussed above shows that Fe^{3+} increases comparably in spinel and in both pyroxenes with increasing temperature. Consequently, the partitioning of Fe^{3+} between pyroxene and spinel is approximately independent of temperature. As previously shown (Canil *et al.*, 1994), whole-rock Fe^{3+} does not depend on temperature. Thus it seems likely that these trends are due to the decrease in the modal amount of spinel with increasing temperature, according to the reaction

$$\underset{\text{spinel}}{MgAl_2O_4} + \underset{\text{ortho/clinopyroxene}}{Mg_2Si_2O_6} = \underset{\text{ortho/clinopyroxene}}{MgAl_2SiO_6} + \underset{\text{olivine}}{Mg_2SiO_4}. \qquad (6)$$

Lowering the amount of the $MgAl_2O_4$ component concentrates Fe^{3+} in spinel, and thus (as the pyroxene–spinel distribution coefficients are insensitive to temperature) in the pyroxenes. This could explain the generally lower $Fe^{3+}/\Sigma Fe$ in spinels from slowly cooled, orogenic massif peridotites vs xenoliths noted above.

The trend translates into a positive correlation of calculated $a_{Fe_3O_4}$ with temperature. The lower calculated relative f_{O_2} values (from olivine–orthopyroxene–spinel equilibria; e.g. Woodland *et al.*, 1992) in orogenic peridotites compared with xenoliths would then simply be produced in this way. Unfortunately, there has as yet been no study of the $Fe^{3+}/\Sigma Fe$ ratios of the coexisting pyroxenes from slowly cooled peridotites with which to test this hypothesis.

The distribution of Fe^{3+} in the garnet peridotite facies

Fe^{3+} in garnet and pyroxenes

Fe^{3+} in garnets from garnet peridotite xenoliths were reported by Luth *et al.* (1990). Those workers showed that mantle garnets have a distinctly bimodal distribution of $Fe^{3+}/\Sigma Fe$ ratios, with low-temperature garnet peridotites having $Fe^{3+}/\Sigma Fe < 0{\cdot}07$, and high-temperature garnet lherzolites having $Fe^{3+}/\Sigma Fe > 0{\cdot}10$. The cause of this variation, and the reason for the bimodality of its distribution, have remained obscure. The increased Fe^{3+} in the high-temperature garnets could be due to a redistribution of Fe^{3+} between garnet and pyroxenes as a function of T and/or P at constant whole-rock Fe^{3+}, or to greater Fe^{3+} whole-rock abundance (the high-temperature garnet peridotites are generally enriched in incompatible elements over the low-temperature ones). The bimodal distribution of Fe^{3+} in the garnets may be recording a fundamental

layering in the mantle's redox state (Haggerty, 1990).

The new data of this study do not show the bimodal distribution, but rather suggest a continuous increase of $Fe^{3+}/\Sigma Fe$ (and Fe^{3+}) in garnet with temperature (Fig. 8). Possibly, the bimodality in Fe^{3+} found by Luth *et al.* (1990) simply reflects the bimodality in other properties of garnet peridotite lithosphere sampled by southern African kimberlites. Garnet lherzolite xenoliths from many southern African kimberlites define a discontinuous P–T spectrum, one part populated by the low-temperature, more depleted samples, the other by the high-temperature, 'fertile' and often sheared samples (Boyd, 1973; Boyd & Nixon, 1975; Nixon & Boyd, 1975). In agreement with Luth *et al.* (1990), we can identify no correlation of Fe^{3+} in garnet with any major element (e.g. Ca), such as would indicate some crystal-chemical control on Fe^{3+} substitution.

The pyroxenes of the garnet peridotite facies have $Fe^{3+}/\Sigma Fe$ ratios extending to slightly greater values than those for spinel peridotites (i.e. up to 0·1 for opx, and 0·41 for cpx). The distribution of Fe^{3+} between ortho- and clinopyroxene is the same as that found in spinel lherzolites (Fig. 9). In contrast to the samples from the spinel lherzolite facies, there is only a slight correlation between Fe^{3+} in clinopyroxene and temperature of equilibration (Fig. 10a). This would be expected if the cause of the trend in the former were indeed the decrease in the modal abundance of spinel with increasing temperature, as postulated above. As for the spinel lherzolites, there is no correlation of Fe^{3+} in clinopyroxene with Na (Fig. 10b).

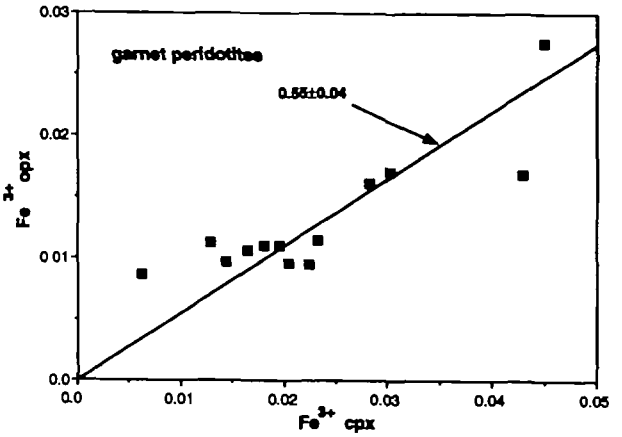

Fig. 9. Correlation of Fe^{3+} cations (based on four cation stoichiometry) in coexisting clino- and orthopyroxenes from garnet peridotites in this study. The correlation is similar to that found in coexisting pyroxenes from the spinel lherzolite facies (Fig. 1). The quoted uncertainty is the standard error of the estimate.

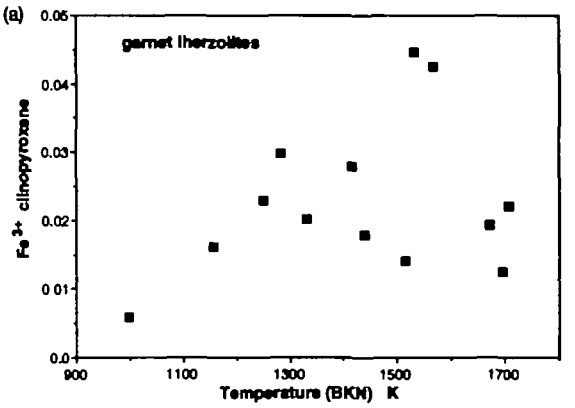

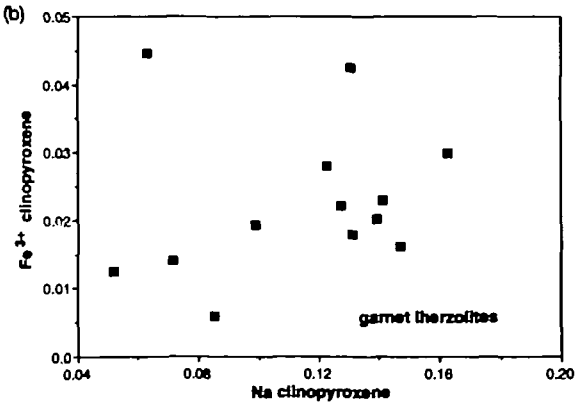

Fig. 10. Variation of Fe^{3+} in clinopyroxene with (a) temperature [T_{BKN}, in Kelvin, calculated using the two-pyroxene geothermometer of Brey & Köhler (1990)] and (b) Na, for garnet peridotites. All data are from this study.

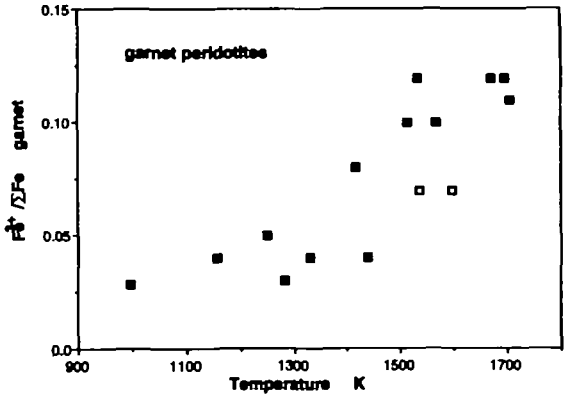

Fig. 8. Variation of $Fe^{3+}/\Sigma Fe$ ratio in garnet with temperature (in Kelvin) for garnet peridotite samples from this study. Closed symbols calculated using the two-pyroxene method of Brey & Köhler (1990), open symbols using the Fe–Mg exchange between olivine and garnet (O'Neill & Wood, 1979).

Partitioning of Fe^{3+} between garnet and pyroxene

Whole-rock Fe_2O_3 in garnet peridotites has no correlation with temperature of equilibration (Fig. 11), demonstrating that the increase of Fe^{3+} in garnet with increasing temperature does not depend on whole-rock Fe_2O_3, and must therefore arise from the redistribution of Fe^{3+} out of the other Fe^{3+}-containing phases (i.e. the pyroxenes), and into the garnet. This effect may be shown by the following semi-quantitative exercise.

If we make use of components for which thermodynamic data are available, the distribution of Fe^{3+} between garnet and clinopyroxene can be represented by the exchange reaction

$$\underset{\text{clinopyroxene}}{NaFe^{3+}Si_2O_6} + 1/2\ \underset{\text{garnet}}{Ca_3Al_2Si_3O_{12}} = \underset{\text{clinopyroxene}}{NaAlSi_2O_6} + 1/2\ \underset{\text{garnet}}{Ca_3Fe^{3+}_2Si_3O_{12}} \quad (7)$$

so that at equilibrium

$$\ln \frac{(a^{gt}_{Ca_3Fe_2Si_3O_{12}})^{1/2}}{a^{cpx}_{NaFeSi_2O_6}} - \ln \frac{(a^{gt}_{Ca_3Al_2Si_3O_{12}})^{1/2}}{a^{cpx}_{NaAlSi_2O_6}} = \frac{-\Delta G^\circ}{RT}. \quad (8)$$

To apply this equation, some simplifying approximations are needed. First, the ΔV° of this reaction is comparatively small (−0·085 J/bar), so for simplicity we will ignore the effect of pressure. Second, we find from our database (Table 2) that the Fe^{3+} concentration in garnet does not depend on Ca content, and similarly that Fe^{3+} in clinopyroxene does not depend on Na in clinopyroxene, and thus we assume that the thermodynamic activities of the $Ca_3Fe^{3+}_2Si_3O_{12}$ and $NaFe^{3+}Si_2O_6$ components depend only on the concentrations of Fe^{3+} in garnet and clinopyroxene, respectively. We can therefore write

$$\ln \frac{(a^{gt}_{Ca_3Fe_2Si_3O_{12}})^{1/2}}{a^{cpx}_{NaFeSi_2O_6}} = \ln D^{gt/cpx}_{Fe^{3+}} + \text{constant}. \quad (9)$$

We assume that $a^{gt}_{Ca_3Al_2Si_3O_{12}}$ is constant in garnet peridotites, being buffered by coexisting orthopyroxene and clinopyroxene. The corresponding assumption that $a^{cpx}_{NaAlSi_2O_6}$ is constant cannot be justified, as this component is the principal host for Na in the peridotite whole rock and thus depends mainly on the degree of depletion. Unfortunately, we cannot take its variation explicitly into account without making a complex statement on activity–composition relations in chemically complex clinopyroxenes, which is beyond the scope of our study. Instead, we shall assume $a^{cpx}_{NaAlSi_2O_6}$ that varies randomly among the samples. These assumptions lead to the following approximate relationship:

$$\ln D^{gt/cpx}_{Fe^{3+}} \approx \frac{-\Delta H^\circ}{RT} + \text{constant}. \quad (10)$$

Thus, in a plot of $\ln D^{gt/cpx}_{Fe^{3+}}$ vs reciprocal temperature (Fig. 12), the slope is given by $-\Delta H^\circ(7)/R$, with variations in $a^{cpx}_{NaAlSi_2O_6}$ as a possible source of scatter. The observed slope from our data is −6·6, implying $\Delta H^\circ = 55$ kJ/mol. This is much higher than the $\Delta H^\circ(7)$ of 7·1 kJ/mol calculated for reaction (7) using the thermodynamic data for all phases from Holland & Powell (1990). Both values of ΔH° confirm the strong temperature dependence of the partitioning of Fe^{3+} between clinopyroxene and

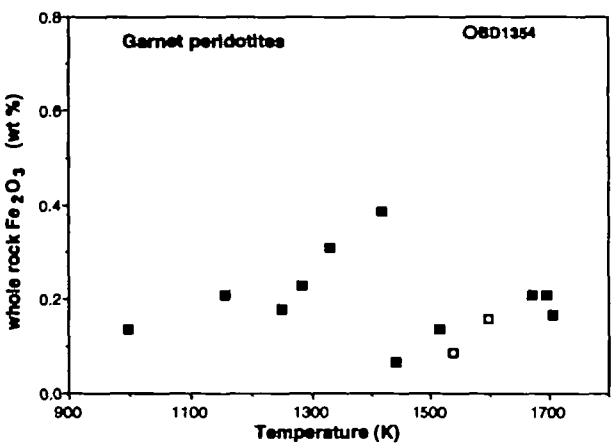

Fig. 11. Whole-rock Fe_2O_3 for garnet peridotites from this study compared with temperature of equilibration, calculated as described in Fig. 10. Data for whole-rock Fe_2O_3 from Table 2 [see also Canil *et al.* (1994)]. [Note that sample BD1354 with high Fe_2O_3 is a garnet pyroxenite, not a peridotite (see Table 1).]

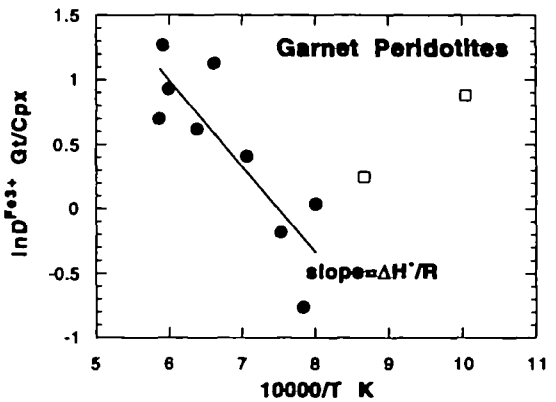

Fig. 12. Plot showing ln $D^{Fe^{3+}}$ Gt/Cpx vs reciprocal temperature for garnet peridotites from this study. The fitted line does not include data for two anomalous samples UV417/89 and FRB1350, which contain ilmenite and spinel, respectively. The fitted line has the equation

$$\ln D^{Fe^{3+}}\text{Gt/Cpx} = 4{\cdot}97 - 0{\cdot}66354/T\ (R = 0{\cdot}85).$$

garnet observed in natural samples, but the magnitude of the ΔH° derived from the natural data is mainly due to ignoring the variable and unknown effect of $a^{cpx}_{NaAlSi_2O_6}$ in our simplification for exchange reaction (7). Nevertheless, the general trend is obvious: that lower temperatures generally favour more substitution of Fe^{3+} into pyroxenes relative to coexisting garnet. The partitioning systematics for Fe^{3+} between pyroxenes and garnet demonstrate that the higher $Fe^{3+}/\Sigma Fe$ in garnets from high-temperature peridotites reported by Luth *et al.* (1990) is simply due to the effect of temperature (see Fig. 14, below) and not necessarily due to elevated bulk Fe_2O_3 contents caused by pre-entrainment metasomatism or oxidation.

IMPLICATIONS FOR THE THERMOBAROMETRY OF GARNET PERIDOTITES

The thermobarometry of mantle-derived garnet peridotites has been a matter of controversy, concerning the formulations used to calculate P–T of equilibration of samples, the resultant shape of derived palaeogeotherms (e.g. Finnerty, 1989; Carswell, 1991), and the state of equilibrium within the actual mineral assemblages to which the thermobarometers have been applied. The equilibrium assumption can be tested either by the convergence of different mineral geothermobarometers to produce the same P–T estimate (e.g. Brey, 1991) or by solution of the inverse chemical equilibrium problem using Duhem's theorem for equilibrium between phases (Nicholls, 1977; Gordon, 1992). The latter method is dependent on solution models for the phases involved, which for chemically complex pyroxenes and Al–Cr–Fe^{3+}-bearing garnets, are very unconstrained (e.g. Luth *et al.*, 1990). Brey's (1991) approach is simpler, but requires that all geothermobarometer combinations be correctly calibrated by experiment.

The data collected in this study provide an opportunity to examine the effect of Fe^{3+} contents of all coexisting mantle minerals on equilibria used to calculate P–T conditions for mantle-derived garnet peridotites. Similar assessments have been made previously for two-pyroxene thermometry (McGuire *et al.*, 1989; Luth & Canil, 1993) and for garnet–olivine thermometry (Luth *et al.*, 1990), but no study has examined the effect of Fe^{3+} in all phases on P–T estimates for the same samples using different thermobarometer combinations. The convergence of temperature estimates for all thermobarometer combinations between these phases may in favourable cases be used for criteria to establish internal mineral equilibrium, and is therefore important in the construction and interpretation of palaeogeotherms. For comparative purposes, however, the following discussion concerns only the thermometer–barometer combinations recommended for the most part by Brey & Köhler (1990) rather than serving as a critique of various published thermobarometric formulations.

A comparison of two-pyroxene temperatures calculated with and without considering Fe^{3+} for garnet peridotites using the two-pyroxene thermometer–Al-in-orthopyroxene barometer formulation (T_{BKN}–P_{BKN}) of Brey & Köhler (1990) shows that Fe^{3+} in ortho- or clinopyroxene has little effect on this thermometer (Fig. 13a), because it does not directly affect the exchange of the $Mg_2Si_2O_6$ component between coexisting pyroxenes on which the thermometer is based (Luth & Canil, 1993). For this reason, it is assumed in the ensuing discussion that T_{BKN} gives reliable temperature estimates and records the 'correct' temperature of equilibration of the samples. For this reason, we used T_{BKN} in our discussion of the temperature dependence of Fe^{3+} partitioning between different phases. All other thermometers are then compared with this temperature. The comparison of T_{BKN} with other thermometers does not, of course, eliminate the possibility of internal disequilibrium.

Fe^{2+}–Mg exchange geothermometers

Assumptions involving the amount of Fe^{3+} in phases directly affect the Fe/Mg ratio used in calculating K_DFe–Mg to derive temperature estimates from Fe^{2+}–Mg exchange geothermometers. A large change in calculated temperature can result from olivine–garnet exchange thermometers (Fig. 13b), depending on whether Fe^{3+} is ignored or explicitly considered in the calculation of Fe/Mg in garnet (Fe^{3+} concentrations of olivine are essentially zero).

In general, better empirical agreement is attained between T_{BKN} and olivine–garnet Fe–Mg exchange thermometry if Fe^{3+} in garnet is ignored, presumably because the experiments used to calibrate the geothermometer produced garnets with similar Fe^{3+} contents to most of the mantle samples. Almost half of the samples studied, however, plot off the 1:1 correlation with T_{BKN} even if Fe^{3+} is ignored (Fig. 13b). The reason for this remains unclear, but could, for example, be caused by re-annealing of these samples at a lower temperature, as Fe^{2+}–Mg exchange reactions are expected to have lower closure temperatures than the two-pyroxene equilibrium. Moreover, Fe^{3+} in orthopyroxene affects P

estimation (discussed below), which in turn affects T estimation with Fe–Mg thermometers.

Unlike olivine–garnet Fe–Mg exchange thermometry, where only one phase hosts significant Fe^{3+}, both phases in the clinopyroxene–garnet Fe–Mg exchange thermometer usually contain significant amounts of Fe^{3+} in mantle-derived samples, and, moreover, the $Fe^{3+}/\Sigma Fe$ in clinopyroxene generally greatly exceeds even that in garnet. This makes the clinopyroxene–garnet Fe–Mg exchange even more sensitive to consideration of Fe^{3+}. Again, the empirical test (Fig. 13c) shows that few clinopyroxene–garnet temperatures are in agreement with T_{BKN} whether Fe^{3+} is ignored or considered in both the garnet and clinopyroxene. Similar but slightly more favourable results are obtained for orthopyroxene–garnet Fe–Mg exchange temperatures (Fig. 13d).

The generally better agreement between T_{BKN} and temperatures from the various Fe–Mg thermometers deployed with all Fe treated as Fe^{2+} (even where the phase concerned has demonstrably high Fe^{3+} contents) implies that the experiments used to calibrate these Fe–Mg exchange thermometers produced garnet and/or clinopyroxene with substantial Fe^{3+} contents, similar to that of the natural samples. This is in fact likely, as the majority of these high-pressure experiments employed graphite capsules. Data for natural samples F556, F865, FRB1350, UV465/86, UV177/89, GP147 and GP87B indicate that significant Fe^{3+} can be present in natural garnets or pyroxenes coexisting with carbon as either graphite or diamond (Table 3). It is clear, however, that the redox state of some samples is not in equilibrium with elemental carbon, and it would be fortuitous if a sample had an identical redox state to that of the experimental calibrations. This must introduce an inaccuracy into Fe^{2+}–Mg exchange geothermometry which cannot be quantified, because the redox conditions of the experiments used to calibrate most Fe–Mg thermometers are not well known (Luth & Canil, 1993). For example, the two garnet–olivine pyroxenite samples from the Western Gneiss Region, Norway (Carswell, 1986; Jamtveit *et*

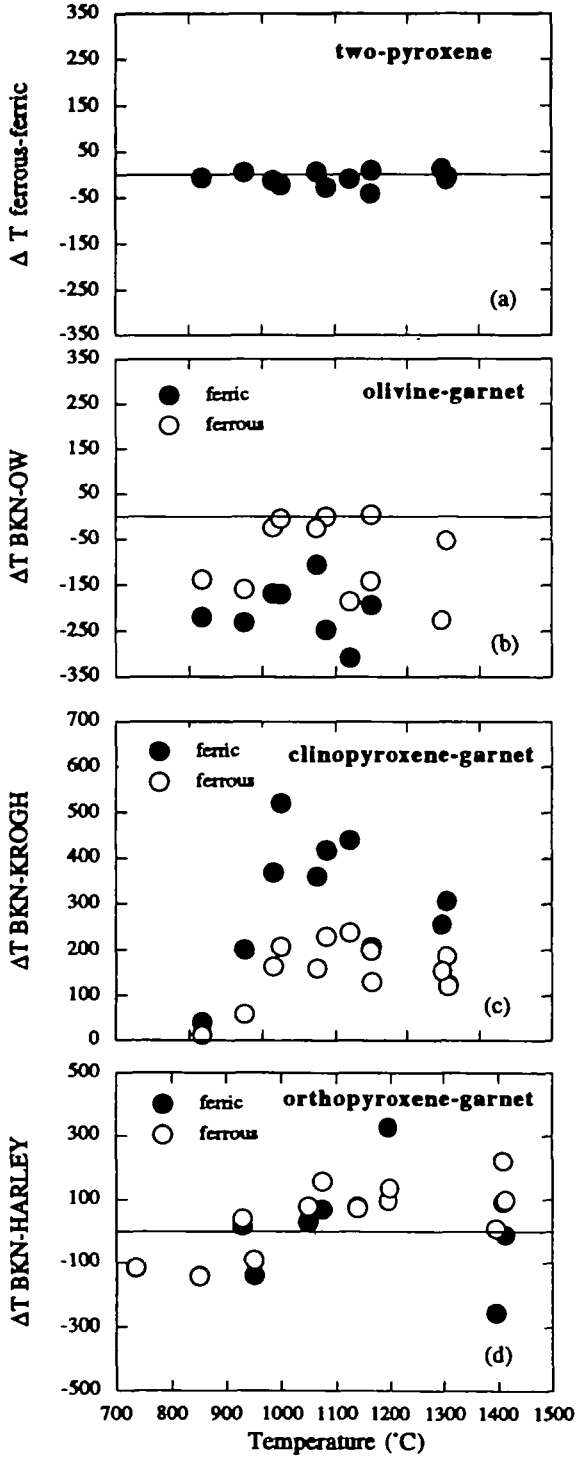

Fig. 13. Comparison of temperature calculated with and without considering Fe^{3+} in phases in the peridotite samples. The two-pyroxene temperature (T_{BKN}) of Brey & Köhler (1990) is assumed to be the 'correct' temperature in the samples, and the comparison with all other thermometers, with and without considering Fe^{3+} present in the phases, is plotted as ΔT. Results are for (a) the two-pyroxene geothermometer (T_{BKN}), (b) olivine–garnet Fe–Mg exchange thermometer (T_{OW}) of O'Neill & Wood (1979), (c) clinopyroxene–garnet Fe–Mg exchange thermometer (T_{KROGH}) of Krogh (1988) and (d) orthopyroxene–garnet thermometer (T_{H84}) of Harley (1984). All of the above thermometers were calculated with pressures determined using the Al-in-Opx barometer P_{BKN} of Brey & Köhler (1990), except that of Harley (1984), which was coupled with the barometer of Nickel & Green (1985). (Note that Fe^{3+} contents were not determined by Mössbauer for some orthopyroxenes and that pressures of 5·0 GPa were assumed in samples lacking orthopyroxene.)

al., 1991) contain garnet, orthopyroxene and clinopyroxene with no detectable Fe^{3+} in their Mössbauer spectra (U95, U539; Table 3). Application of the usual Fe–Mg thermometers, calibrated from Fe^{3+}-bearing experiments, to these Norwegian samples must necessarily produce spurious results.

A lack of convergence of Fe–Mg exchange thermometers on the same P–T value as derived from T_{BKN} should not by itself be used as evidence for internal disequilibrium in the sample considered, but rather may reflect different amounts of Fe^{3+} in the natural samples from those in the experimental calibration. The concentrations of Fe^{3+} in the experiments used to calibrate Fe–Mg exchange thermometers are themselves not known, which prohibits the application of any quantitative corrections. Finally, we have shown that the partitioning of Fe^{3+} between phases in the natural samples can depend on temperature, a phenomenon which could result in errors of calculated temperature that change systematically with temperature. In summary, Fe–Mg exchange thermometers are highly suspect, and conclusions derived from them must be treated with caution, including their use as empirical calibrants for other geothermometers. In particular, eclogites pose great problems for accurate geothermometry, as temperature estimates for these rocks are entirely dependent on the highly susceptible clinopyroxene–garnet Fe–Mg exchange thermometer.

Geobarometry using Al in orthopyroxene in equilibrium with garnet

Currently, estimates of pressures of equilibration in garnet peridotites are based on the equilibrium between orthopyroxene and garnet:

$$\underset{\text{orthopyroxene}}{MgAl_2SiO_6} + \underset{\text{orthopyroxene}}{Mg_2Si_2O_6} = \underset{\text{garnet}}{Mg_3Al_2Si_3O_{12}}. \quad (11)$$

In contrast to the situation for geothermometry, there are few usable alternatives to this equilibrium for estimating pressures. Thus the determination of mantle palaeogeotherms (Boyd, 1973) is almost entirely dependent on this equilibrium.

The effect of Fe^{3+} on this equilibrium is not directly obvious, as it is in Fe–Mg exchange geothermometry. It arises from the effect which Fe^{3+} may have on the calculation of the activity of the $MgAl_2SiO_6$ component in orthopyroxene. This component consists of Al substituting for Mg in the M1 octahedral site, charge balanced by Al for Si in the tetrahedral sites. Typical orthopyroxenes from garnet peridotites have 0·4–1·2 wt% Al_2O_3 (e.g. Table 2), corresponding to 0·02–0·05 atoms per formula unit of six oxygens. The present results show that these orthopyroxenes also contain 0·007–0·015 atoms Fe^{3+} per formula unit, with similar quantities of Cr^{3+}, so that typically the atomic $(Fe^{3+} + Cr^{3+})$ in orthopyroxenes is nearly equal to atomic Al (and occasionally exceeds it, as in sample 89-669). The larger size of the Fe^{3+} and Cr^{3+} ions, and the excess crystal field stabilization energy of Cr^{3+} in octahedral sites, suggests that these ions will preferentially substitute into the M1 octahedral site, which would necessitate equal amounts of Al charge-balancing in the tetrahedral sites. Given the observed proportions of $(Fe^{3+} + Cr^{3+})$ relative to Al, this kind of substitution obviously has the potential to limit the amount of Al available for substituting into the M1 octahedral site, and thus to reduce the calculated activity of the $MgAl_2SiO_6$ component, perhaps drastically. All that can be said at present is that the $a_{MgAl_2SiO_6}$ must remain finite, even where atomic $(Fe^{3+} + Cr^{3+}) > Al$. This suggests that a complex order–disorder model for the 3+ cations on the M1 and tetrahedral sites may be required to describe the thermochemical properties of natural pyroxenes adequately. At present, the extent of the error produced by ignoring Fe^{3+} (and Cr^{3+}) in calculating $a_{MgAl_2SiO_6}$ remains completely unconstrained.

CAN ACCURATE MINERAL $Fe^{3+}/\Sigma Fe$ RATIOS BE CALCULATED FROM STOICHIOMETRY?

The above discussion indicates a general need for accurate estimation of Fe^{3+}/Fe^{2+} in mantle minerals, if accurate geothermobarometry is to be attempted. The time-consuming technique of mineral separation and Mössbauer spectroscopy employed here is realistically only likely to be able to satisfy this need for a small minority of samples. This raises the question of whether accurate $Fe^{3+}/\Sigma Fe$ ratios can be determined by other, more routine, methods.

$Fe^{3+}/\Sigma Fe$ ratios can also be estimated from chemical analyses [usually electron microprobe (EMP) analyses], by assuming charge balance and perfect stoichiometry. Wood & Virgo (1989) have shown empirically by comparison with Mössbauer results that this method works well for spinels, provided that adequate standards and correction procedures are used.

By contrast, for garnets and pyroxenes, experience shows that $Fe^{3+}/\Sigma Fe$ values calculated from stoichiometry often vary widely. The scatter of $Fe^{3+}/\Sigma Fe$ determinations from microprobe data might indicate that this method would never produce

reliable results (e.g. Dyar *et al.*, 1989). The empirical failure of EMP analyses to give reasonable $Fe^{3+}/\Sigma Fe$ ratios, however, could also mean inadequate EMP procedures had been used, rather than that the EMP method is necessarily too imprecise. This question has not yet been explicitly addressed.

We have therefore calculated the 'statistically most probable stoichiometric formulae', together with their root mean square (r.m.s.) errors, as a function of $Fe^{3+}/\Sigma Fe$ ratios, according to the method of Dollase & Newman (1984). We imposed the constraints of charge balance, perfect stoichiometry with complete occupancy of all cation and anion sites (i.e. 3 cations to 4 oxygens for spinels, 4 cations to 6 oxygens for pyroxenes, and 8 cations to 12 oxygens for garnets), and totals to add to 100 wt%. As explained by Dollase & Newman (1984), the statistical validity of this method depends on knowledge of the standard deviations of the measured concentrations of each oxide component. Here we assume that the EMP analyses contain no systematic errors, so that these standard deviations result from counting statistics. With this assumption, we obtained estimates of standard deviations for the major oxide components (MO_x) relevant to the major mantle minerals, as a function of concentration according to the relation

$$\sigma_{MO_x} = A + B c_{MO_x} \qquad (12)$$

which was suggested by Dollase & Newman (1984). C_{MO_x} is the amount of oxide (wt%). Input data were the theoretical values of σ_{MO_x} from a large number of actual EMP analyses of pyroxenes, garnets, spinels, feldspars and olivines, performed on a Cameca SX50 microprobe at the Bayerisches Geoinstitut (Bayreuth, Germany) using standard operating conditions in wavelength-dispersive (WDS) mode (15 kV, 15 nA, counting times 20 s on peaks, 10 s on each side of the background). Values of A and B for each oxide are given in Table 4. Such a set of values is only an example, for longer counting times will produce better statistics, as will multiple analyses on a homogeneous mineral grain. As a convenient point of reference, the uncertainty in a SiO_2 analysis at 50 wt% SiO_2 would be $\pm 0{\cdot}26$, one standard deviation.

Results of the Dollase–Newman calculation for a representative spinel, garnet and clinopyroxene are given in Fig. 14. The r.m.s. error is a parabolic function of $Fe^{3+}/\Sigma Fe$, and has two features of importance: (1) the minimum, corresponding to the best estimate of $Fe^{3+}/\Sigma Fe$ by this method, and (2) the slopes on either side of this minimum. The latter feature, which is the quantity of interest in this discussion, depends on the standard deviations of the component oxides. The former, the minimum, is a measure of how near the analysis is to one that would give perfect stoichiometry, and is therefore also subject to systematic errors, such as poorly known or inappropriate standards, or errors in the correction procedure, which we have not taken into account. It is noteworthy, however, that in all three cases (and in the many others we have examined),

Table 4: Estimated errors in electron microprobe (EMP) analyses

Oxide	Standard deviation [$A + B$(wt% oxide)]
MgO	$0{\cdot}02 + 0{\cdot}005MgO$
Al_2O_3	$0{\cdot}03 + 0{\cdot}004Al_2O_3$
Na_2O	$0{\cdot}02 + 0{\cdot}010Na_2O$
K_2O	$0{\cdot}01 + 0{\cdot}008K_2O$
Cr_2O_3	$0{\cdot}02 + 0{\cdot}007Cr_2O_3$
CaO	$0{\cdot}02 + 0{\cdot}006CaO$
FeO	$0{\cdot}07 + 0{\cdot}005FeO$
SiO_2	$0{\cdot}01 + 0{\cdot}005SiO_2$
NiO	$0{\cdot}02 + 0{\cdot}009NiO$

Other oxides were treated as the nearest one of the above in the periodic table with similar valence (e.g. MnO as FeO).

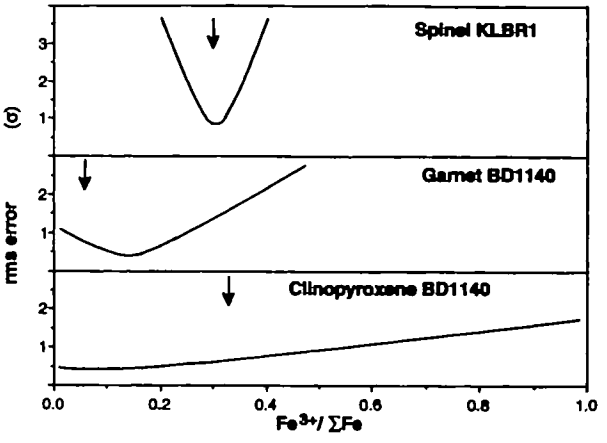

Fig. 14. Root mean square (r.m.s.) error as a function of $Fe^{3+}/\Sigma Fe$ for a representative upper-mantle spinel, garnet and clinopyroxene, assuming standard deviations for the measured concentrations of the oxide components given in Table 4. Analyses for spinel from Canil *et al.* (1990) and for garnet and clinopyroxene from Carswell & Dawson (1970). Arrows mark $Fe^{3+}/\Sigma Fe$ ratios determined by Mössbauer spectroscopy [this study and Canil *et al.* (1990)]. Wet chemical analysis of $Fe^{3+}/\Sigma Fe$ in garnet BD1140 by Carswell & Dawson (1970) gave 0·15, vs 0·06 by Mössbauer. When compared with Mössbauer spectroscopy, wet chemical analyses of refractory minerals and whole-rock peridotites give inflated values of $Fe^{3+}/\Sigma Fe$ [see O'Neill *et al.* (1993) and Canil *et al.* (1994)].

the analyses do in fact conform within reasonable error (2σ) to the stoichiometric ideal.

For the spinel analysis, the slopes of the r.m.s. error vs $Fe^{3+}/\Sigma Fe$ are very steep. The width of the parabola at a particular value of σ is an estimate of the uncertainty in $Fe^{3+}/\Sigma Fe$. As a convenient approximation, the width at 2σ can be taken to be four times the standard deviation in $Fe^{3+}/\Sigma Fe$. In this way, the estimated standard deviation in $Fe^{3+}/\Sigma Fe$ for this spinel is 0·025. This is a similar level of accuracy to that found for $Fe^{3+}/\Sigma Fe$ in spinels by Wood & Virgo (1989), and identical to that observed empirically by comparison with Mössbauer measurements by Woodland *et al.* (1992). This agreement suggests that our estimate of the standard deviations of the component oxides is reasonable. Within their combined uncertainties, the EMP estimate of $Fe^{3+}/\Sigma Fe$ is identical to that from Mössbauer spectroscopy (0·30). This shows that our EMP procedures have been accurate, as well as precise.

The situation for garnet and pyroxene is not so encouraging. The value of σ ($Fe^{3+}/\Sigma Fe$) for a representative garnet (from sample BD1140) is 0·12, whereas that for a clinopyroxene (also BD1140) is 0·53. As the total range of $Fe^{3+}/\Sigma Fe$ for mantle garnets (excluding the Norwegian samples with zero $Fe^{3+}/\Sigma Fe$; Tables 2 and 3) is 0·02–0·13, and for clinopyroxenes is 0·12–0·41, this level of imprecision is too large to be petrologically useful. At best, if the precision can be improved by a factor of four, for example by doing more than 16 replicate analyses on a homogeneous phase, it may be possible to distinguish between low-temperature garnets with $Fe^{3+}/\Sigma Fe < 0·07$ and high-temperature garnets with $Fe^{3+}/\Sigma Fe > 0·10$, provided, of course, that systematic errors are eliminated through use of calibrated garnet standards.

The greater imprecision of the $Fe^{3+}/\Sigma Fe$ estimates for garnets and pyroxenes compared with those for spinels is a result of lower total Fe, much higher levels of SiO_2 and the effect of the uncertainty in SiO_2 in propagating through the stoichiometry calculation. The effect of these factors increases in the order spinel > garnet > pyroxene. Finally, it should be remembered that the assumption of perfect stoichiometry is known not to hold for some mantle clinopyroxenes from high-temperature eclogites (McCormick, 1986).

CONCLUSIONS

The upper mantle's complement of ferric iron is distributed fairly homogeneously amongst all anhydrous phases in both garnet and spinel peridotites, with the important exception of olivine, which contains negligible Fe^{3+}. This distribution has no correlation with bulk-rock Fe_2O_3 content, or f_{O_2}. Although whole-rock Fe_2O_3 contents have a simple inverse correlation with the degree of depletion (Canil *et al.*, 1994), the complexity of the interphase partitioning for Fe^{3+} results in complicated variations of the activities of Fe^{3+}-bearing components, and hence of calculated equilibrium f_{O_2} values.

In spinel peridotites, spinel has high $Fe^{3+}/\Sigma Fe$, high FeO* (mostly 11–16 wt %) but low modal abundance (1–2%), orthopyroxene has low $Fe^{3+}/\Sigma Fe$, moderate FeO* (4–8 wt %) and high modal abundance (20–25%), whereas clinopyroxene has high $Fe^{3+}/\Sigma Fe$, low FeO* (1·4–4 wt %) and can have high modal abundance (~15% in the most primitive samples, but decreasing with degree of depletion). The net result is that all three phases contribute approximately similar amounts to the whole-rock Fe_2O_3. In this way, Fe_2O_3 differs from the majority of the other incompatible minor and trace elements in peridotites, which are either concentrated into clinopyroxene (e.g. Na and the rare earth elements: McDonough *et al.*, 1992) or shared between clino- and orthopyroxene (e.g. Ti: Rampone *et al.*, 1991; McDonough *et al.*, 1992).

The decrease of Fe_2O_3 in mantle peridotites with increasing degree of depletion (Canil *et al.*, 1994) is similar to that exhibited by trace elements with similarly equable intra-crystalline distributions between the major upper-mantle phases, such as Sc, Ga and V (e.g. Frey *et al.*, 1986). Thus, Fe^{3+} behaves as a moderately incompatible component during the partial melting of mantle peridotite, with an empirical melt–residue partition coefficient of ~0·1 (O'Neill *et al.*, 1993; Canil *et al.*, 1994). This value of $D_{Fe^{3+}}^{liq/sol}$ is similar to that of Ga, a trace element with generally similar geochemical properties to Fe^{3+} in the mantle regime (e.g. McKay & Mitchell, 1988). The simple depletion trend of Fe^{3+} in most mantle samples shows that melt extraction from these samples occurred under conditions in which oxygen is not a mobile phase. That is, f_{O_2} reflects rather than controls bulk-rock $Fe^{3+}/\Sigma Fe$.

Ferric iron can, however, vary more widely than expected from this simple trend in mantle-derived magmas (Carmichael, 1991). This is presumably because Fe^{3+} concentrations also reflect any changes in the oxygen content of the system, which may occur not only through mantle metasomatism of the source region, but also from magma degassing. Considered as a trace element, Fe^{3+} potentially exhibits behaviour of special interest because it is sensitive to open-system processes involving oxygen, whereas it is less sensitive than most elements (because of its equitable partitioning behaviour) to the details of

partial melting or fractional crystallization, which often dominate other trace element abundances.

The distribution of Fe^{3+} between clinopyroxene and garnet in the garnet peridotite facies is shown to be strongly temperature dependent. Increasing temperature (and pressure) favours substitution of Fe^{3+} out of the pyroxenes and into coexisting garnet. This partitioning relationship explains the high $Fe^{3+}/\Sigma Fe$ in garnets from high-temperature sheared peridotite xenoliths in kimberlite. For this reason, the higher $Fe^{3+}/\Sigma Fe$ in garnets from these samples are not indicative of higher whole-rock oxygen contents and/or interaction with more oxidized metasomatic fluid.

The major source of uncertainty in thermobarometry with regard to Fe^{3+} in most natural garnet peridotites lies in the lack of knowledge of Fe^{3+} concentrations both in natural phases and in the phases from which the thermobarometers were calibrated in the original laboratory experiments. Two-pyroxene geothermometry is nearly immune to this problem, and will give the most reliable results for both spinel and garnet peridotite assemblages. In so far as pressure estimates still depend on the Al-in-orthopyroxene geobarometer, however, the real effect of Fe^{3+} on reconstructed upper-mantle palaeogeotherms is still not known. Because of the inaccuracies of Fe–Mg exchange thermometry in Fe^{3+}-bearing samples, internal mineral equilibrium cannot be accurately tested using the agreement of different thermobarometers.

Statistical analysis of electron microprobe estimates for Fe^{3+} concentrations in mantle phases shows that the greater imprecision of the $Fe^{3+}/\Sigma Fe$ estimates for garnets and pyroxenes compared with those for spinels results from lower total Fe, much higher levels of SiO_2 and the uncertainty in SiO_2. In the case of garnet, it may be possible to obtain sufficiently precise electron microprobe analyses for the accurate determination of $Fe^{3+}/\Sigma Fe$ if proper standards are available, and if the minerals are sufficiently chemically homogeneous to allow large numbers of replicate analyses, but the situation looks pessimistic for pyroxenes.

ACKNOWLEDGEMENTS

The authors are very grateful to D. A. Carswell, R. Rudnick, W. F. McDonough, D. G. Pearson, F. R. Boyd, P. H. Nixon and N. Pokhilenko for generously providing samples, mineral chemical data and petrographic information required to carry out this investigation. Reviews by D. Eggler, C. Ballhaus and an anonymous referee are appreciated. The written portion of this research was supported in part by NSERC of Canada grants to D. Canil.

REFERENCES

Amthauer, G., Annersten, H. & Hafner, S. S., 1976. The Mössbauer spectrum of ^{57}Fe in silicate garnets. *Zeitschrift für Kristallographie* **143**, 14–55.

Annersten, H., Olesch, M. & Seifert, F. A., 1978. Ferric iron in orthopyroxene: a Mössbauer spectroscopic study. *Lithos* **11**, 301–310.

Ballhaus, C., Berry, R. F. & Green, D. H., 1991. High pressure experimental calibration of the olivine–orthopyroxene–spinel oxygen geobarometer: implications for the oxidation state of the upper mantle. *Contributions to Mineralogy and Petrology* **107**, 27–40.

Boyd, F. R., 1973. A pyroxene geotherm. *Geochimica et Cosmochimica Acta* **37**, 2533–2546.

Boyd, F. R. & Mertzman, S. A., 1987. Composition and structure of the Kaapvaal lithosphere, South Africa. In: Mysen, B. O. (ed.) *Magmatic Processes: Physicochemical Principles. Geochemical Society Special Publication* **1**, 13–24.

Boyd, F. R. & Nixon, P. H., 1975. Origins of the ultramafic nodules from some kimberlites of Northern Lesotho and the Monastery Mine, South Africa. *Physics and Chemistry of the Earth* **9**, 431–544.

Boyd, F. R., Pearson, D. G., Pokhilenko, N. P. & Mertzman, S. A., 1993. Cratonic mantle composition: evidence from Siberian xenoliths. *EOS* **74**, 321.

Brey, G., 1991. Fictive conductive geotherms beneath the Kaapvaal craton. (abstract). *Extended Abstracts, 5th International Kimberlite Conference, Araxa, Brazil*. Rio de Janeiro: CPRM Special Publication 2/91, pp. 23–25.

Brey, G. & Köhler, T., 1990. Geothermometry in four phase lherzolites II. New thermobarometers, and practical assessment of existing thermobarometers. *Journal of Petrology* **31**, 1353–1378.

Bryndzia, L. T. & Wood, B. J., 1990. Oxygen thermobarometry of abyssal spinel peridotites: the redox state and C–O–H volatile composition of the Earth's suboceanic upper mantle. *American Journal of Science* **290**, 1093–1116.

Canil, D., Virgo, D. & Scarfe, C. M., 1990. Oxidation states of mantle xenoliths from British Columbia, Canada. *Contributions to Mineralogy and Petrology* **104**, 453–562.

Canil, D., O'Neill, H. St. C., Pearson, D. G., Rudnick, R. L., McDonough, W. F. & Carswell, D. A., 1994. Ferric iron in peridotites and mantle oxidation states. *Earth and Planetary Science Letters* **123**, 205–220.

Carmichael, I. S. E., 1991. The oxidation state of basic magmas: a reflection of their source regions? *Contributions to Mineralogy and Petrology* **106**, 129–142.

Carswell, D. A., 1986. The metamorphic evolution of Mg–Cr type Norwegian garnet peridotites. *Lithos* **19**, 279–297.

Carswell, D. A., 1991. The garnet–orthopyroxene Al barometer: problematic application to natural garnet lherzolite assemblages. *Mineralogical Magazine* **55**, 19–31.

Carswell, D. A. & Dawson, J. B., 1970. Garnet peridotite xenoliths in South African kimberlite pipes and their petrogenesis. *Contributions to Mineralogy and Petrology* **25**, 163–184.

Cosca, M. A. & Peacor, D. R., 1987. Chemistry and structure of esseneite, $CaFeAlSiO_6$, a new pyroxene produced by pyrometamorphism. *American Mineralogist* **72**, 148–156.

Dawson, J. B. & Smith, J. V., 1988. Metasomatized and veined upper mantle xenoliths from Pello Hill, Tanzania: evidence for anomalously light mantle beneath the Tanzanian sector of the East African Rift valley. *Contributions to Mineralogy and Petrology* **100**, 510–527.

Dollase, W. A., 1975. Statistical limitations of Mössbauer spectral fitting. *American Mineralogist* **60,** 257–264.

Dollase, W. A. & Newman, W. I., 1984. Statistically most probable stoichiometric formulae. *American Mineralogist* **69,** 553–556.

Dyar, M. D., McGuire, A. V. & Ziegler, R. D., 1989. Redox equilibria and chemistry of coexisting minerals from spinel lherzolite mantle xenoliths. *American Mineralogist* **74,** 969–980.

Dyar, M. D., McGuire, A. V. & Harrell, M. D., 1992. Crystal chemistry of two styles of metasomatism in the upper mantle. *Geochimica et Cosmochimica Acta* **56,** 2579–2586.

Finnerty, A. A., 1989. Xenolith-derived mantle geotherms: whither the inflection? *Contributions to Mineralogy and Petrology* **102,** 367–375.

Frey, F. A. & Green, D. H., 1974. The mineralogy, geochemistry and origin of lherzolite inclusions in Victorian basanites. *Geochimica et Cosmochimica Acta* **38,** 1023–1059.

Frey, F. A., Suen, C. J. & Stockman, H. W., 1986. The Ronda high temperature peridotite: geochemistry and petrogenesis. *Geochimica et Cosmochimica Acta* **49,** 2469–2491.

Gordon, T. M., 1992. Generalized thermobarometry: solution of the inverse geochemical problem using data for individual species. *Geochimica et Cosmochimica Acta* **56,** 1793–1800.

Green, D. H. & Ringwood, A. E., 1967. The stability fields of aluminous pyroxene peridotite and garnet peridotite and their relevance in upper mantle structure. *Earth and Planetary Science Letters* **3,** 151–160.

Haggerty, S. E., 1990. Redox state of the continental lithosphere. In: Menzies, M. A. (ed.) *Continental Mantle*. Oxford: Clarendon Press, pp. 87–109.

Harley, S. L., 1984. An experimental study of the partitioning of Fe and Mg between garnet and orthopyroxene. *Contributions to Mineralogy and Petrology* **86,** 359–373.

Holland, T. J. B. & Powell, R., 1990. An enlarged and updated internally consistent thermodynamic dataset with uncertainties and correlations: the system K_2O–Na_2O–CaO–MgO–MnO–FeO–Fe_2O_3–Al_2O_3–TiO_2–SiO_2–C–H_2–O_2. *Journal of Metamorphic Geology* **8,** 89–124.

Huckenholz, H. G., Schairer, J. F. & Yoder, H. S., Jr, 1969. Synthesis and stability of ferri-diopside. *Mineralogical Society of America Special Paper* **2,** 163–177.

Ionov, D. A. & Wood, B. J., 1993. The oxidation state of subcontinental mantle: oxygen thermobarometry of mantle xenoliths from central Asia. *Contributions to Mineralogy and Petrology* **111,** 179–193.

Irvine, T. N., 1965. Chromian spinel as a petrogenetic indicator: Part I, Theory. *Canadian Journal of Earth Sciences* **2,** 648–672.

Jamtveit, B., Carswell, D. A. & Mearns, E. W., 1991. Chronology of the high pressure metamorphism of Norwegian garnet peridotites/pyroxenites. *Canadian Journal of Earth Sciences* **9,** 125–139.

Kinzler, R. & Grove, T. L., 1992. Primary magmas of mid-ocean ridge basalts. 1. Experiments and methods. *Journal of Geophysical Research* **97,** 6885–6906.

Krogh, E. J., 1988. The garnet–clinopyroxene Fe–Mg geothermometer—a reinterpretation of existing experimental data. *Contributions to Mineralogy and Petrology* **99,** 44–48.

Luth, R. W. & Canil, D., 1993. Ferric iron in mantle-derived pyroxenes and a new oxybarometer for the upper mantle. *Contributions to Mineralogy and Petrology* **113,** 236–248.

Luth, R. W., Virgo, D., Boyd, F. R. & Wood, B. J., 1990. Ferric iron in mantle derived garnets: implications for thermobarometry and for the oxidation state of the mantle. *Contributions to Mineralogy and Petrology* **104,** 56–72.

McCormick, T. C., 1986. Crystal chemical aspects of nonstoichiometric pyroxenes. *American Mineralogist* **71,** 1434–1440.

McDonough, W. F. & McCulloch, M. T., 1987. The southeast Australian lithospheric mantle: isotopic and geochemical constraints on its growth and evolution. *Earth and Planetary Science Letters* **86,** 327–340.

McDonough, W. F., Stosch, H.-G. & Ware, N., 1992. Distribution of titanium and the rare earth elements between peridotitic minerals. *Contributions to Mineralogy and Petrology* **110,** 321–328.

McGuire, A. V., Dyar, M. D. & Ward, K. A., 1989. Neglected Fe^{2+}/Fe^{3+} ratios: a study of the Fe^{3+} content of megacrysts from alkali basalts. *Geology* **17,** 687–690.

McGuire, A. V., Dyar, M. D. & Nielson, J. E., 1991. Metasomatic oxidation of upper mantle peridotite. *Contributions to Mineralogy and Petrology* **109,** 252–264.

McKay, D. B. & Mitchell, R. H., 1988. Abundance and distribution of gallium in some spinel and garnet lherzolites. *Geochimica et Cosmochimica Acta* **52,** 2867–2870.

Nicholls, J., 1977. The calculation of mineral compositions and modes of olivine–two pyroxene–spinel assemblages. *Contributions to Mineralogy and Petrology* **60,** 119–142.

Nickel, K. G. & Green, D. H., 1985. Empirical thermobarometry for garnet peridotites and implications for the nature of the lithosphere, kimberlites and diamonds. *Earth and Planetary Science Letters* **73,** 158–170.

Nixon, P. H. & Boyd, F. R., 1975. Petrogenesis of the granular and sheared ultrabasic nodule suite in kimberlites. In: Nixon, P. H. (ed.) *Lesotho Kimberlites*. Maseru: Lesotho National Development Corporation, pp. 48–56.

O'Neill, H. St. C. & Wall, V. J., 1987. The olivine–orthopyroxene–spinel oxygen geobarometer, the nickel precipitation curve, and the oxygen fugacity of the Earth's upper mantle. *Journal of Petrology* **28,** 1169–1191.

O'Neill, H. St. C. & Wood, B. J., 1979. An experimental study of Fe–Mg partitioning between garnet and olivine and its calibration as a geothermometer. *Journal of Petrology* **70,** 59–70.

O'Neill, H. St. C., Rubie, D. C., Canil, D., Geiger, C., Ross, C. R. II, Seifert, F. & Woodland, A. B., 1993. Ferric iron in the upper mantle and in transition zone assemblages: implications for relative oxygen fugacities in the mantle. In: *Evolution of the Earth and Planets. Geophysical Monograph, American Geophysical Union* **74,** IUGG Volume 14, 73–88.

Ottonello, G., Piccardo, G. B. & Mazzucotelli, A., 1978. Clinopyroxene–orthopyroxene major and rare earth element partitioning in spinel peridotite xenoliths from Assab, Ethiopia. *Geochimica et Cosmochimica Acta* **42,** 1817–1828.

Pearson, D. G., Davies, G. R. & Nixon, P. H., 1993. Geochemical constraints on the petrogenesis of diamond facies pyroxenites from the Beni Bousera peridotite massif, north Morocco. *Journal of Petrology* **34,** 125–172.

Pearson, D. G., Boyd, F. R., Haggerty, S. E., Pasteris, J. D., Field, S. W., Nixon, P. H. & Pokhilenko, N. P., 1994. The characterization and origin of graphite in cratonic lithospheric mantle: a petrological, carbon isotope and Raman spectroscopic study. *Contributions to Mineralogy and Petrology* **115,** 449–463.

Pearson, D. G., Shirey, S. B., Carlson, R. W., Boyd, F. R., Pokhilenko, N. P. & Shimizu, N., 1995. Re–Os, Sm–Nd and Rb–Sr isotope evidence for thick Archean lithospheric mantle beneath the Siberian craton modified by multi-stage metasomatism. *Geochimica et Cosmochimica Acta* **59,** 959–971.

Pokhilenko, N. P., Pearson, D. G., Boyd, F. R. & Sobolev, N. V., 1991. Megacrystalline dunites and peridotites: sources of Siberian diamonds. *Carnegie Institution of Washington, Yearbook* 11–18.

Rampone, E., Bottazi, P. & Ottolini, L., 1991. Complementary Ti and Zr anomalies in orthopyroxenes and clinopyroxenes from mantle peridotites. *Nature* **354,** 518–520.

Rudnick, R. J., McDonough, W. F. & Orpin, A., 1992. Northern Tanzanian peridotite xenoliths: a comparison with Kaapvaal peridotites and inferences on metasomatic interactions. In: Meyer, H. O. A. & Leonardos, O. (eds) *Kimberlites, Related Rocks and Mantle Xenoliths, Vol. I. Proceedings of the 5th International Kimberlite Conference*, Brasilia: CPRM Publishing, pp. 336–353.

Rudnick, R. J., McDonough, W. F. & Chappell, B. W., 1993. Carbonatite metasomatism in the northern Tanzanian mantle: petrographic and geochemical characteristics. *Earth and Planetary Science Letters* **114,** 463–475.

Sachtleben, Th. & Seck, H. A., 1981. Chemical control of Al-solubility in orthopyroxene and its implications on pyroxene geothermometry. *Contributions to Mineralogy and Petrology* **78,** 157–165.

Seifert, F., 1983. Mössbauer line broadening in aluminous orthopyroxenes: evidence for next-nearest neighbour interactions and short range order. *Neues Jahrbuch für Mineralogie, Abhandlungen* **148,** 141–162.

Shee, S. R., Gurney, J. J. & Robinson, D. N., 1982 Two diamond-bearing peridotite xenoliths from the Finsch kimberlite, South Africa. *Contributions to Mineralogy and Petrology* **81,** 79–87.

Viljoen, K. S., Swash, P. M., Otter, M. L., Schulze, D. J. & Lawless, P. J., 1992. Diamondiferous garnet harzburgites from the Finsch kimberlite, North Cape, South Africa. *Contributions to Mineralogy and Petrology* **110,** 133–138.

Walter, M. J. & Presnall, D. C., 1994. Melting behavior of simplified lherzolite in the system CaO–MgO–Al_2O_3–SiO_2–Na_2O from 7 to 35 kbar. *Journal of Petrology* **35,** 329–359.

Wood, B. J. & Nicholls, J., 1977. The thermodynamics of reciprocal solid solutions. *Contributions to Mineralogy and Petrology* **66,** 389–400.

Wood, B. J. & Virgo, D., 1989. Upper mantle oxidation state: ferric iron contents of lherzolite spinels by ^{57}Fe Mössbauer spectroscopy and resultant oxygen fugacities. *Geochimica et Cosmochimica Acta* **53,** 1277–1291.

Woodland, A. B., Kornprobst, J. & Wood, B. J., 1992. Oxygen thermobarometry of orogenic lherzolite massifs. *Journal of Petrology* **33,** 203–330.

RECEIVED JUNE 1, 1995
REVISED TYPESCRIPT ACCEPTED JANUARY 1, 1996

APPENDIX: ^{57}Fe MOSSBAUER FITTING PROCEDURES

Examples of Mössbauer spectra fitted using the models described below are shown in Fig. A1.

Olivine

Spectra for olivines were fitted with two symmetric, quadrupole split doublets for Fe^{2+}. No Fe^{3+} was detected in any of the olivines studied.

Pyroxene

Orthopyroxene spectra were fitted with three symmetric, quadrupole split doublets for Fe^{2+} and one symmetric, quadrupole split doublet for Fe^{3+}. Other fitting models have been used in the literature (e.g. Seifert, 1983), but change in the fitting model did not alter the $Fe^{3+}/\Sigma Fe$ ratio, which ranges from 0·03 to 0·10. At $Fe^{3+}/\Sigma Fe$ ratios below 0·05, orthopyroxene spectra could be fitted equally well with $Fe^{3+}/\Sigma Fe$ ranging from 0·02 to 0·05, and in many cases, it was required to constrain the $Fe^{3+}/\Sigma Fe$ ratio to obtain a fit with reasonable hyperfine parameters for Fe^{3+} [i.e. isomer shift (IS) >0, full width at half-height (FWHH) $<0·8$]. For spectra with very small but recognizable contributions of Fe^{3+} to the resonance envelope, the tendency was to fit much of the background in the spectrum, sometimes producing unreasonably low IS (<0 mm/s) and high FWHH ($\leqslant 2·0$ mm/s). For this reason, orthopyroxene spectra were first fitted with fixed $Fe^{3+}/\Sigma Fe$ ($\sim 0·05$), and then this constraint was released until convergence with reasonable IS and FWHH values was attained. It follows that the $Fe^{3+}/\Sigma Fe$ ratios determined for orthopyroxenes at levels below $\sim 0·05$ are probably not very accurate.

Clinopyroxene spectra were fitted with two symmetric, quadrupole split doublets for Fe^{2+} and one symmetric, quadrupole split doublet for Fe^{3+}. More complicated fitting models for Ca-rich clinopyroxene involving doublets for both tetrahedral and octahedral Fe^{3+} in the clinopyroxene structure can be adopted (i.e. McGuire *et al.*, 1991), but given the uncertainty in resolving two distinct doublets under the high-velocity shoulder of the low-velocity peak in these spectra [see Dollase (1975)] such fits are considered here to be unwarranted.

Both ortho- and clinopyroxenes from garnet-bearing assemblages generally have lower FWHH for Fe^{2+} compared with pyroxenes from the spinel lherzolite facies (Table 3). This effect is attributed to the higher Al contents of pyroxenes from the spinel-bearing assemblages (Table 2), which produce significant next nearest neighbour effects, and line broadening for Fe^{2+} in the spectra (Seifert, 1983). It is possible to adequately fit most orthopyroxene spectra from the garnet-bearing assemblages with only one or two doublet models for Fe^{2+}, but as noted above, alteration of the original three doublet model for Fe^{2+} did not affect the resultant $Fe^{3+}/\Sigma Fe$ ratio. For consistency, all orthopyroxene spectra were fitted using the same model.

Spinel

Spinel spectra were fitted as was done by Wood & Virgo (1989), with two symmetric, quadrupole split doublets for Fe^{2+} and one symmetric, quadrupole split doublet for Fe^{3+}.

Garnet

Garnet spectra were fitted using the approach of Luth *et al.* (1990), which uses one asymmetric doublet for Fe^{2+} and one symmetric doublet for Fe^{3+}. In 80 K spectra, significant line broadening of the Fe^{2+} peaks is observed such that spectra could be fitted with equal statistical quality using a model with two symmetric doublets for Fe^{2+}. Fits with two symmetric doublets for Fe^{2+} resulted in the same $Fe^{3+}/\Sigma Fe$ ratio. As in orthopyroxene, there is a significant amount of uncertainty associated with $Fe^{3+}/\Sigma Fe$ ratios of garnets at levels below $\sim 0·05$, owing to poor resolution of the contribution of Fe^{3+} to the resonance envelope in spectra recorded at 80 K (Luth *et al.*, 1990).

Phlogopite and amphibole

Spectra for amphibole and phlogopite were fitted with two or three symmetric, quadrupole split doublets for Fe^{2+} and one symmetric, quadrupole split doublet for Fe^{3+}. Changes in fitting model for either phase did not alter the resultant $Fe^{3+}/\Sigma Fe$ ratio derived from the Mössbauer spectra (Table 3).

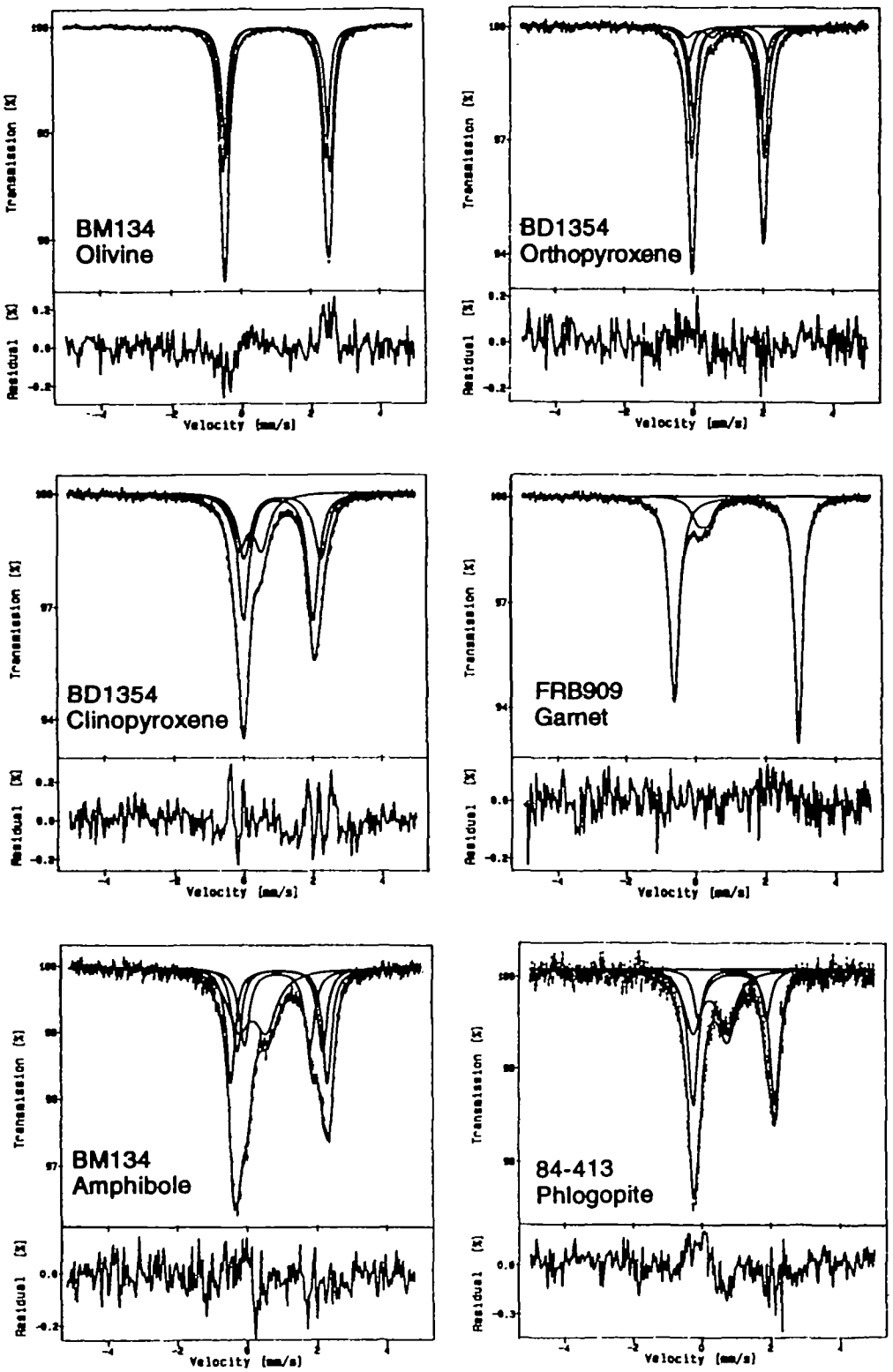

Fig. A1. Examples of fitted Mössbauer spectra collected at 298 K for olivine, orthopyroxene, clinopyroxene, garnet, amphibole and phlogopite. Descriptions of the fitting models are given in the Appendix.